

1    **OPERATOR SPLITTING/FINITE ELEMENT METHODS FOR THE  
2    MINKOWSKI PROBLEM\***

3    HAO LIU<sup>†</sup>, SHINGYU LEUNG<sup>‡</sup>, AND JIANLIANG QIAN<sup>§</sup>

4    **Abstract.** The classical Minkowski problem for convex bodies has deeply influenced the development of differential geometry. During the past several decades, abundant mathematical theories have been developed for studying the solutions of the Minkowski problem; however, the numerical solution of this problem has been largely left behind, with only a few methods available to achieve that goal. In this article, focusing on the two-dimensional Minkowski problem with Dirichlet boundary conditions, we introduce two solution methods, both based on operator-splitting. One of these two methods deals directly with the Dirichlet condition, while the other one uses an approximation à la Robin of this Dirichlet condition. The relaxation of the Dirichlet condition makes the second method better suited than the first one to treat those situations where the Minkowski equation (of the Monge–Ampère type) and the Dirichlet condition are not compatible. Both methods are generalizations of the solution method for the canonical Monge–Ampère equation discussed by Glowinski et al. (A Finite Element/Operator-Splitting Method for the Numerical Solution of the Two Dimensional Elliptic Monge–Ampère Equation, *Journal of Scientific Computing*, 79(1), 1–47, 2019); as such they take advantage of a divergence formulation of the Minkowski problem, which makes it well-suited to both a mixed finite-element approximation and the time-discretization via an operator-splitting scheme of an associated initial value problem. Our methodology can be easily implemented on convex domains of rather general shape (with curved boundaries, possibly). The numerical experiments validate both methods, showing that if one uses continuous piecewise affine finite element approximations of the solution of the Minkowski problem and of its three second order derivatives, these two methods provide nearly second-order accuracy for the  $L^2$  and  $L^\infty$  norms of the approximation error, where the Minkowski–Dirichlet problem is assumed to have a smooth solution. One can extend easily the methods discussed in this article, to address the solution of three-dimensional Minkowski problems.

27    **Key words.** operator-splitting methods, Minkowski problem, Monge–Ampère equation, mixed  
28    finite element methods

29    **MSC codes.** 65N30,65M60

30    **1. Introduction.** The Minkowski problem (named after Hermann Minkowski  
31    (1864–1909)) is an important problem in Differential Geometry. It asks for the construction  
32    of a compact surface  $S$  as boundary of a convex bounded domain, knowing  
33    its Gaussian curvature. Given a compact strictly convex hypersurface  $S$  in the  $d$ –  
34    dimensional real space  $\mathbb{R}^d$ , the Gauss map  $\mathbf{G}$  is a diffeomorphism from  $S$  to the unit  
35    sphere  $\mathbf{S}^{d-1}$  of  $\mathbb{R}^d$ . Map  $\mathbf{G}$  is defined by  $\mathbf{G}(\mathbf{x}) = \mathbf{n}(\mathbf{x}), \forall \mathbf{x} \in S$ , where  $\mathbf{n}(\mathbf{x})$  denotes  
36    the unit outward normal of  $S$  at  $\mathbf{x}$ . Accordingly, the Gauss–Kronecker curvature  $K$  is  
37    the Jacobian of the Gauss map. Minkowski stated that one has

38    (1.1)    
$$\int_{\mathbf{S}^{d-1}} \mathbf{x} (K(\mathbf{G}^{-1}(\mathbf{x})))^{-1} d\sigma(\mathbf{x}) = \mathbf{0},$$

---

\*Submitted to the editors DATE.

**Funding:** Hao Liu was partially supported by National Natural Science Foundation of China 12201530, HKRGC ECS 22302123, HKBU 179356. Shingyu Leung was partially supported by the Hong Kong RGC under grant 16302223. Jianliang Qian was partially funded by NSF 2012046, 2152011, and 2309534.

<sup>†</sup>Department of Mathematics, Hong Kong Baptist University, Kowloon Tong, Hong Kong (haoliu@hkbu.edu.hk).

<sup>‡</sup>Department of Mathematics, The Hong Kong University of Science and Technology, Clear Water Bay, Hong Kong (masyleung@ust.hk).

<sup>§</sup>Department of Mathematics and Department of CMSE, Michigan State University, East Lansing, MI 48824, U.S.A. (jqian@msu.edu).

39 where  $\sigma$  is the Lebesgue measure on  $\mathbf{S}^{d-1}$ . Conversely, Minkowski posed the following  
 40 (inverse) problem: Suppose that  $f$  is a strictly positive function defined over  $\mathbf{S}^{d-1}$   
 41 verifying  $\int_{\mathbf{S}^{d-1}} \mathbf{x} f(\mathbf{x}) d\sigma(\mathbf{x}) = \mathbf{0}$ ; can one find a hypersurface  $S$  having  $1/f$  as Gaussian  
 42 curvature? In [41, 42], Minkowski discussed the existence and uniqueness of solutions  
 43 to the above inverse problem. For  $d = 2$ , the solution regularity was proved by Lewy  
 44 [33, 34], Nirenberg [44], and Pogorelov [45], while, for  $d > 2$ , the solution regularity  
 45 was analyzed by Cheng and Yau [11] and Pogorelov [46].

46 Despite being around for more than a century and being one of the most important  
 47 problems in Differential Geometry, not much was done concerning the numerical  
 48 solution of the Minkowski problem. The earliest attempt we could find was discussed  
 49 in [36, 37], two publications dedicated to the solution of a related problem: namely,  
 50 reconstructing a shape from extended Gaussian images. In [31], after generalizing  
 51 Minkowski's proof, Lamberg converted the Minkowski problem into an optimization  
 52 one, the resulting algorithm solving a polyhedral version of the Minkowski problem.  
 53 In [32], Lamberg introduced an algorithm based on Minkowski's isoperimetric inequality,  
 54 leading to an approximate Minkowski problem taking place in a finite-dimensional  
 55 function space spanned by truncated spherical harmonic series. In a more recent publication [10],  
 56 Cheng designed a level-set based finite-difference PDE method to drive  
 57 an implicitly defined surface towards shapes arising from the Minkowski problem.

58 In all the above cited works the hypersurface is supposed to be closed. Actually, another type of Minkowski problem is the Minkowski–Dirichlet problem. For  
 59 the Minkowski–Dirichlet problem, one supposes that the hypersurface is open and  
 60 bounded, with a Dirichlet condition imposed on its boundary. The well-posedness of  
 61 this problem has been addressed by many authors: For example, Bakelman [3], Lions  
 62 [35] and Urbas [50, 51, 52] have proved the existence and uniqueness of a solution.  
 63 Trudinger and Urbas [48] proved a necessary and sufficient condition for the classical  
 64 solvability of the Minkowski–Dirichlet problem. Recently, in [30] Hamfett designed  
 65 a monotone finite-difference method to solve the Minkowski–Dirichlet problem; since  
 66 the method relies on wide stencils, it is advantageous for those situations where, due  
 67 to the lack of classical solutions, one looks for viscosity solutions.

68 Here, we propose two new methods for the numerical solution of the Minkowski–  
 69 Dirichlet problem in dimension  $d = 2$ . The first method, well suited to problems with  
 70 classical solutions, imposes the Dirichlet condition in a strong sense. On the other  
 71 hand, the second method imposes the Dirichlet condition in a least-squares sense (via  
 72 a quadratic penalty technique), making it appropriate for those situations where, due  
 73 to data incompatibility, the Minkowski–Dirichlet problem has no solution. Of course,  
 74 the second method has also the ability to capture classical solutions, if such solutions  
 75 do exist. The Minkowski problem we will look at can be described as follows: Let  $\Omega$   
 76 be a bounded domain of  $\mathbb{R}^d$  and  $K$  be a positive function defined over  $\Omega$ , and let  $g$  be  
 77 a function defined on the boundary  $\partial\Omega$ ; can one find a function  $u$  defined over  $\Omega$  and  
 78 verifying  $u|_{\partial\Omega} = g$ , such that  $K$  is the Gauss curvature of the graph of  $u$  (a surface in  
 79  $\mathbb{R}^{d+1}$ )? In partial differential equation form, the above Minkowski–Dirichlet problem  
 80 reads as follows:

$$82 \quad (1.2) \quad \begin{cases} \frac{\det(\mathbf{D}^2 u)}{(1+|\nabla u|^2)^{1+d/2}} = K & \text{in } \Omega, \\ u = g & \text{on } \partial\Omega. \end{cases}$$

83 The partial differential equation in (1.2) belongs to a family of Monge–Ampère equa-  
 84 tions. The simplest element of this family is clearly the following canonical Monge–

85 Ampère equation

86 (1.3)  $\det(\mathbf{D}^2u) = f \text{ in } \Omega.$

87 Equation (1.3) is elliptic if  $f > 0$ . The above Monge–Amperère equation (1.3) is a  
 88 fully nonlinear second order partial differential equation; it has been drawing a lot of  
 89 attention lately, mostly because its relations with optimal transport problems (other  
 90 applications are described in, e.g., [19]; see also the references therein). During the  
 91 past three decades, a variety of methods have been designed to solve numerically  
 92 equation (1.3), completed by boundary conditions (mostly Dirichlet's) (some of these  
 93 methods are described in the review article [19]). As expected, most of these methods  
 94 focus on the two-dimensional Monge–Ampère equation and cover a large variety of  
 95 approaches. Combinations of (mixed) finite element approximations and augmented  
 96 Lagrangian or least-squares formulations have been applied to the solution of (1.3)  
 97 and related fully nonlinear elliptic equations such as Pucci's (see [4, 8, 13, 15, 14, 17,  
 98 18, 16, 26, 29, 25, 43, 9, 19] for details). Alternative finite-difference and finite-element  
 99 methods have been developed for these fully nonlinear elliptic equations as well; see  
 100 [1, 5, 6, 7, 21, 20, 40, 47, 28, 38, 19], this list being far from complete.

101 The main goal of this article is to extend to problem (1.2) (assuming  $d = 2$ ), the  
 102 operator-splitting based methods developed in [28, 38] for the solution of equation  
 103 (1.3) (completed by Dirichlet conditions) in dimensions 2 and 3 and in [27, 39] for  
 104 the eigenvalue problems of (1.3). Following [28, 38], the first step in that direction is  
 105 to take advantage of a divergence formulation of problem (1.2), better suited to finite  
 106 element approximations. The second step is to decouple (in some sense) differential  
 107 operators and nonlinearities by introducing as additional unknown functions  $\mathbf{p} = \mathbf{D}^2u$   
 108 (as done in [27, 38]) and  $\mathbf{s} = \nabla u$  (which was not necessary in [27, 38]). At the end of  
 109 the second step, one has replaced the highly nonlinear scalar Minkowski equation by  
 110 an equivalent system of linear and nonlinear equations for  $u$ ,  $\mathbf{p}$  and  $\mathbf{s}$ , whose formalism  
 111 is simpler. In the third step, we associate an initial value problem (IVP) with the  
 112 above system and use operator-splitting to time-discretize the above IVP, in order to  
 113 capture its steady state solution(s). We use simple finite-element approximations of  
 114 the mixed type to implement the above methodology: indeed, we use finite-element  
 115 spaces of continuous piecewise affine functions to approximate  $u$  and its three second-  
 116 order derivatives, making our methods well-suited to solve problem (1.2) on domains  
 117  $\Omega$  with curved boundaries.

118 As mentioned above we will develop two new methods for the solution of problem  
 119 (1.2): these two methods are very close to each other, the first one dealing directly with  
 120 the boundary condition  $u = g$  on  $\partial\Omega$ , while the second one imposing the boundary  
 121 condition in a least-squares sense.

122 This article is organized as follows: In Section 2, we state some theoretical results  
 123 on the existence and uniqueness of solutions to the Minkowski–Dirichlet problem (1.2).  
 124 In Section 3, we provide the divergence formulation of problem (1.2) and associate  
 125 with it two initial value problems, which differ by the way the Dirichlet boundary  
 126 condition is treated. The time discretization of these two initial value problems by  
 127 operator-splitting is discussed in Section 4, followed by their finite-element space  
 128 discretization in Section 5. We address in Section 6 the initialization of the two above  
 129 algorithms. In Section 7, we report the results of numerical experiments validating  
 130 our methodology. Section 8 concludes the article.

131 **2. Problem formulation, existence, uniqueness and regularity results.**

132 We defined the Minkowski problem in Section 1. In this article, we will focus on the

133 numerical solution of the Minkowski–Dirichlet problem (1.2), assuming that  $d = 2$   
 134 (2-D). A first step to that goal is to rewrite (1.2) as

135 (2.1) 
$$\begin{cases} \det(\mathbf{D}^2u) = K(1 + |\nabla u|^2)^{1+d/2} & \text{in } \Omega, \\ u = g & \text{on } \partial\Omega, \end{cases}$$

136 a Monge–Ampère type formulation, better suited for numerical solution. In (2.1),  $K$   
 137 ( $> 0$ ) is the prescribed curvature and  $\mathbf{D}^2u = \left(\frac{\partial^2 u}{\partial x_i \partial x_j}\right)_{1 \leq i, j \leq d}$  is the Hessian matrix  
 138 of function  $u$ .

139 To put our computational investigations into perspective, we recall some classical  
 140 results concerning the existence, uniqueness and regularity of classical solutions to  
 141 problem (2.1). In [48], one proves the following results about existence and uniqueness.

142 THEOREM 2.1. *Suppose that in (2.1),  $\Omega$  is a uniformly bounded convex domain  
 143 of  $\mathbb{R}^d$ , its boundary  $\partial\Omega$  having  $C^{1,1}$ -regularity. Then, problem (2.1) has, for any  
 144  $g \in C^{1,1}(\bar{\Omega})$ , a unique solution in  $C^2(\Omega) \cap C^{0,1}(\bar{\Omega})$ , if and only if*

145 (2.2) 
$$\int_{\Omega} K dx < \omega_d,$$

146 and

147 (2.3) 
$$K = 0 \text{ on } \partial\Omega.$$

148 The constant  $\omega_d$  in (2.2) is given by  $\omega_d = \int_{\mathbb{R}^d} \frac{d\xi}{(1+|\xi|^2)^{1+d/2}}$  (implying  $\omega_2 = \pi$  and  
 149  $\omega_3 = 4\pi/3$ ); actually,  $\omega_d$  is the volume of the unit ball of  $\mathbb{R}^d$ .

150 Condition (2.3) is required to make sure that a solution exists for arbitrary  $g$ . It  
 151 is proved in [48] that if  $K$  does not vanish on the boundary, one can find a smooth  
 152 function  $g$  such that problem (2.1) has no solution.

153 In [50, 51, 52], one discusses regularity of the solution in the critical case defined  
 154 by

155 (2.4) 
$$\int_{\Omega} K dx = \omega_d,$$

156 where the following results are proved.

157 THEOREM 2.2. *Let  $\Omega$  be a uniformly convex domain of  $\mathbb{R}^d$  with a  $C^{2,1}$  smooth  
 158 boundary, and  $K$  be a positive  $C^2$  smooth function verifying (2.4). If  $u$  is a solution  
 159 of the Minkowski–Dirichlet (2.1), then*

- 160 (i)  $u \in C^{0,1/2}(\Omega)$ ;
- 161 (ii) the graph of  $u$  is  $C^{2,\alpha}$ -smooth for some  $\alpha \in (0, 1)$ ;
- 162 (iii)  $u|_{\partial\Omega}$  is  $C^{1,\alpha}$ -smooth;
- 163 (iv) if  $\partial\Omega$  is  $C^{k+1,\alpha}$  and  $K \in C^{k-1,\alpha}$  with  $k \geq 2$ , then the graph of  $u$  is  $C^{k+1,\alpha}$ -  
 164 smooth and  $u|_{\partial\Omega}$  is  $C^{k+1,\alpha}$ -smooth.

165 See [49] for more details on the solution of the Minkowski problem.

166 Some of the conditions in the above two theorems are rather restrictive and/or  
 167 not easy to verify. Nevertheless, the results they are reporting are very useful from  
 168 two perspectives: on one hand, they suggest test problems, where we know in advance  
 169 that solutions exist; on the other hand, they also suggest some other examples, where  
 170 the answer to existence will be indicated by the results of our computations. Finally,  
 171 we will also consider test problems with known solutions so as to check how fast and  
 172 how accurately our methods recover them.

173     **3. Divergence formulations of the 2-D Minkowski problem and relax-**  
 174     **ation by penalty of the Dirichlet condition.**

175     **3.1. Synopsis.** There are cases where the data  $K$  and  $g$  do not allow the exis-  
 176     tence of classical smooth solutions to problem (2.1). In [30], one introduces a notion of  
 177     viscosity solution to problem (2.1), with the solution satisfying the generalized Monge-  
 178     Ampère equation in [2], but not necessarily the Dirichlet condition. In the following  
 179     sub-sections, we will consider two divergence formulations of problem (2.1) in dimen-  
 180     sion two to enforce the Dirichlet condition. The first formulation keeps the Dirichlet  
 181     condition as it is and is well-suited to those situations where problem (2.1) has clas-  
 182     sical solutions. On the other hand, the second formulation makes use of penalty to  
 183     relax the Dirichlet condition; for large values of the penalty parameter, one recovers  
 184     accurately classical solutions if such solutions do exist, or generalized solutions in the  
 185     absence of classical solutions.

186     **3.2. A first divergence formulation of the 2-D Minkowski-Dirichlet**  
 187     **problem.** If  $d = 2$ , problem (2.1) enjoys the following equivalent formulation (in  
 188     the sense of distributions):

189     (3.1)     
$$\begin{cases} -\nabla \cdot (\text{cof}(\mathbf{D}^2 u) \nabla u) + 2K(1 + |\nabla u|^2)^2 = 0 & \text{in } \Omega, \\ u = g & \text{on } \partial\Omega, \end{cases}$$

where matrix  $\text{cof}(\mathbf{D}^2 u)$  is the cofactor matrix of Hessian  $\mathbf{D}^2 u$ , that is

$$\text{cof}(\mathbf{D}^2 u) = \begin{pmatrix} \frac{\partial^2 u}{\partial x_2^2} & -\frac{\partial^2 u}{\partial x_1 \partial x_2} \\ -\frac{\partial^2 u}{\partial x_1 \partial x_2} & \frac{\partial^2 u}{\partial x_1^2} \end{pmatrix}.$$

190     Problem (3.1) is equivalent to

191     (3.2)     
$$\begin{cases} \begin{cases} -\nabla \cdot (\text{cof}(\mathbf{p}) \nabla u) + 2K(1 + |\mathbf{s}|^2)^2 = 0 & \text{in } \Omega, \\ u = g & \text{on } \partial\Omega, \end{cases} \\ \begin{cases} \mathbf{p} - \mathbf{D}^2 u = \mathbf{0} & \text{in } \Omega, \\ \mathbf{s} = \nabla u & \text{in } \Omega. \end{cases} \end{cases}$$

192     In order to avoid possible troubles at those points of  $\bar{\Omega}$  where  $K$  may vanish, we  
 193     approximate system (3.2) by

194     (3.3)     
$$\begin{cases} \begin{cases} -\nabla \cdot ((\varepsilon \mathbf{I} + \text{cof}(\mathbf{p})) \nabla u) + 2K(1 + |\mathbf{s}|^2)^2 = 0 & \text{in } \Omega, \\ u|_{\partial\Omega} = g & \text{on } \Omega, \end{cases} \\ \begin{cases} \mathbf{p} - \mathbf{D}^2 u = \mathbf{0}, \\ \mathbf{s} - \nabla u = \mathbf{0}, \end{cases} \end{cases}$$

195     with  $\varepsilon$  a small positive parameter. We used successfully this type of regularization  
 196     in [28], for the solution of the canonical Monge-Ampère equation (1.3) completed  
 197     by Dirichlet boundary conditions. In practice, we will use a piecewise linear finite-  
 198     element basis and take  $\varepsilon$  of the order of  $h^2$ ,  $h$  being a space discretization step. Such  
 199     a choice makes the scheme stable while providing optimal second-order accuracy.

200     To solve system (3.3) we are going to associate with it the following initial value

201 problem

$$202 \quad (3.4) \quad \begin{cases} \begin{aligned} & \frac{\partial u}{\partial t} - \nabla \cdot ((\varepsilon \mathbf{I} + \text{cof}(\mathbf{p})) \nabla u) + 2K(1 + |\mathbf{s}|^2)^2 = 0 & \text{in } \Omega \times (0, +\infty), \\ & u|_{\partial\Omega} = g & \text{on } \partial\Omega \times (0, +\infty), \end{aligned} \\ \begin{aligned} & \frac{\partial \mathbf{p}}{\partial t} + \gamma_1 (\mathbf{p} - \mathbf{D}^2 u) = \mathbf{0} & \text{in } \Omega \times (0, +\infty), \\ & \frac{\partial \mathbf{s}}{\partial t} + \gamma_2 (\mathbf{s} - \nabla u) = \mathbf{0} & \text{in } \Omega \times (0, +\infty), \\ & (u(0), \mathbf{p}(0), \mathbf{s}(0)) = (u_0, \mathbf{p}_0, \mathbf{s}_0), \end{aligned} \end{cases}$$

203 to be time-discretized by operator-splitting (in Section 4.1). In (3.4),  $\gamma_1$  and  $\gamma_2$  are  
 204 two positive coefficients chosen so that the smooth modes of  $\mathbf{p}$  and  $\mathbf{s}$  evolve in time  
 205 roughly at the same speed as that of  $u$ . Roughly speaking, the evolution speed of  $u$   
 206 is controlled by the eigenvalue of  $-\nabla^2 u$  and the eigenvalue of  $\mathbf{p} \approx \mathbf{D}^2 u$ . According  
 207 to (2.1), if the eigenvalues of  $\mathbf{D}^2 u$  are close to each other, then they are in the order  
 208 of  $\sqrt{K}$ . Following [28], we advocate defining  $\gamma_1$  and  $\gamma_2$  by

$$209 \quad \gamma_1 = \beta_1 \lambda_0 (\varepsilon + \sqrt{\alpha}), \\ 210 \quad \gamma_2 = \beta_2 \lambda_0 (\varepsilon + \sqrt{\alpha}),$$

211 where  $\lambda_0$  is the smallest eigenvalue of operator  $-\nabla^2$  in  $H_0^1(\Omega)$ ,  $\alpha$  is the lower bound  
 212 of  $K$ , and  $\beta_1$  and  $\beta_2$  are two constants of order one.

213 We comment in passing that we have used and will continue to use the notation  
 214  $\phi(t)$  for the function  $x \rightarrow \phi(x, t)$ . In Section 6, we will discuss the initialization of  
 215 system (3.4).

216 **3.3. A divergence formulation of the 2-D Minkowski-Dirichlet problem  
 217 with relaxation of the boundary condition.** Theorem 2.1 implies that problem  
 218 (2.1) may have no solution, unless function  $K$  belongs to a very specific class of  
 219 functions. In order to deal with such no-solution scenarios as well as we can, we are  
 220 going to relax the boundary condition  $u = g$  using a penalty technique of the least-  
 221 squares type. If problem (2.1) has a classical solution, we expect to recover it when  
 222 the penalty parameter converges to  $+\infty$ .

223 The simplest way to proceed is to start from the following variational formulation  
 224 verified (formally) by any solution  $u$  of problem (2.1):

$$225 \quad (3.5) \quad \begin{cases} u \in H^1(\Omega), \\ \int_{\Omega} (\text{cof}(\mathbf{D}^2 u) \nabla u) \cdot \nabla v dx + 2 \int_{\Omega} K(1 + |\nabla u|^2)^2 v dx = 0, \quad \forall v \in H_0^1(\Omega), \\ u = g \text{ on } \partial\Omega. \end{cases}$$

226 In order to relax the Dirichlet boundary condition, we are going to apply to problem  
 227 (3.5) the well-known penalty method discussed in [23, 24] to approximate Dirichlet's  
 228 problems for linear second-order elliptic operators by Robin's ones.

229 Let  $\kappa$  be a positive constant. We (formally) approximate the variational problem  
 230 (3.5) by

$$231 \quad (3.6) \quad \begin{cases} u \in H^1(\Omega), \\ \int_{\Omega} (\text{cof}(\mathbf{D}^2 u) \nabla u) \cdot \nabla v dx + 2 \int_{\Omega} K(1 + |\nabla u|^2)^2 v dx + \\ \kappa \int_{\partial\Omega} (u - g) v d\Gamma = 0, \quad \forall v \in H^1(\Omega), \end{cases}$$

232 where coefficient  $\kappa$  acts as a weight, controlling the level of penalization. Some remarks  
 233 are in order.

234     Remark 3.1. Let us consider the functional  $j_2 : H^1(\Omega) \rightarrow \mathbb{R}$  defined by

235     
$$j_2(v) = \frac{\kappa}{2} \int_{\partial\Omega} |v - g|^2 d\Gamma, \quad \forall v \in H^1(\Omega).$$

236     Functional  $j_2$  is convex and  $C^\infty$  over  $H^1(\Omega)$ , its differential  $Dj_2(v)$  at  $v$  being given  
237     by

238     (3.7)     
$$\langle Dj_2(v), w \rangle = \kappa \int_{\partial\Omega} (v - g) w d\Gamma, \quad \forall v, w \in H^1(\Omega),$$

239     where  $\langle \cdot, \cdot \rangle$  denotes a duality pairing between  $(H^1(\Omega))'$  (the dual space of  $H^1(\Omega)$ )  
240     and  $H^1(\Omega)$ . Consequently, we can identify  $Dj_2(u)$  with  $\kappa(u|_{\partial\Omega} - g)$  and replace  
241      $\kappa \int_{\partial\Omega} (u - g) v d\Gamma$  in (3.6) by  $\langle Dj_2(u), v \rangle$ .

242     Remark 3.2. If a function  $u$  is a solution of the nonlinear variational problem  
243     (3.6), it is also a solution (in the sense of distributions) of the following (fully nonlin-  
244     ear) boundary value problem

245     (3.8)     
$$\begin{cases} -\nabla \cdot (\text{cof}(\mathbf{D}^2 u) \nabla u) + 2K(1 + |\nabla u|^2)^2 = 0 & \text{in } \Omega, \\ \frac{1}{\kappa} (\text{cof}(\mathbf{D}^2 u) \nabla u) \cdot \mathbf{n} + u = g & \text{on } \partial\Omega, \end{cases}$$

246     where, in (3.8),  $\mathbf{n}$  denotes the unit outward normal vector at  $\partial\Omega$ . The boundary  
247     condition in (3.8) is a (nonlinear) *Robin* boundary condition. When  $\kappa \rightarrow +\infty$ , prob-  
248     lem (3.8) ‘converges’ (formally) to problem (2.1), justifying our second divergence  
249     formulation of problem (2.1).

250     Remark 3.3. A natural alternative to problem (3.6) is the one described by

251     (3.9)     
$$\begin{cases} u \in H^1(\Omega), \\ \int_{\Omega} (\text{cof}(\mathbf{D}^2 u) \nabla u) \cdot \nabla v dx + 2 \int_{\Omega} K(1 + |\nabla u|^2)^2 v dx + \\ \langle \partial j_1(u), v \rangle = 0, \quad \forall v \in H^1(\Omega), \end{cases}$$

252     where, in (3.9),  $\partial j_1(u)$  is the sub-differential at  $u$  of the convex Lipschitz continuous  
253     functional  $j_1 : H^1(\Omega) \rightarrow \mathbb{R}$ , defined by

254     
$$j_1(v) = \kappa \int_{\partial\Omega} |v - g| d\Gamma, \quad \forall v \in H^1(\Omega).$$

255     This type of  $L^1$  functional is very common in *Non-Smooth Mechanics* and increasingly  
256     popular in *Data Science* as shown by various chapters of [29].

257     Proceeding as in Section 3.2, we associate with (3.6) the semi-variational system  
(3.10)

258     
$$\begin{cases} u \in H^1(\Omega), \\ \int_{\Omega} \left( \left( \frac{1}{2} \varepsilon \mathbf{I} + \text{cof}(\mathbf{p}) \right) \nabla u \right) \cdot \nabla v dx + \int_{\Omega} \frac{1}{2} \varepsilon \nabla u \cdot \nabla v dx \\ \quad + 2 \int_{\Omega} K(1 + |\mathbf{s}|^2)^2 v dx + \kappa \int_{\partial\Omega} (u - g) v d\Gamma = 0, \quad \forall v \in H^1(\Omega), \\ \mathbf{p} - \mathbf{D}^2 u = \mathbf{0}, \\ \mathbf{s} - \nabla u = \mathbf{0}, \end{cases}$$

259     where in the second row,  $\int_{\Omega} \left( \frac{1}{2} \varepsilon \mathbf{I} \right) \nabla u \cdot \nabla v dx + \int_{\Omega} \frac{1}{2} \varepsilon \nabla u \cdot \nabla v dx (= \int_{\Omega} \varepsilon \nabla u \cdot \nabla v dx)$  is the  
260     regularization term with a role similar to  $\nabla \cdot ((\varepsilon \mathbf{I}) \nabla u)$  in (3.3). The next step is to

261 associate with (3.10) an initial value problem, as we have done with (3.3) in Section  
 262 3.2. The initial value problem reads as:

$$263 \quad (3.11) \quad \begin{cases} u(t) \in H^1(\Omega), \forall t > 0, \\ \int_{\Omega} \frac{\partial u}{\partial t} v dx + \int_{\Omega} \left[ \frac{1}{2} \varepsilon I + \text{cof}(\mathbf{p}) \right] \nabla u \cdot \nabla v dx + \int_{\Omega} \frac{1}{2} \varepsilon \nabla u \cdot \nabla v dx \\ \quad + 2 \int_{\Omega} K(1 + |\mathbf{s}|^2)^2 v dx + \kappa \int_{\partial\Omega} (u - g) v d\Gamma = 0, \quad \forall v \in H^1(\Omega), \\ \frac{\partial \mathbf{p}}{\partial t} + \gamma_1(\mathbf{p} - \mathbf{D}^2 u) = \mathbf{0} \text{ in } \Omega \times (0, +\infty), \\ \frac{\partial \mathbf{s}}{\partial t} + \gamma_2(\mathbf{s} - \nabla u) = \mathbf{0} \text{ in } \Omega \times (0, +\infty), \\ (u(0), \mathbf{p}(0), \mathbf{s}(0)) = (u_0, \mathbf{p}_0, \mathbf{s}_0). \end{cases}$$

264 As in Section 3.2, we advocate taking

$$265 \quad \gamma_1 = \beta_1 \lambda_0 (\varepsilon + \sqrt{\alpha}), \\ 266 \quad \gamma_2 = \beta_2 \lambda_0 (\varepsilon + \sqrt{\alpha}).$$

267 In Section 6, we will discuss the initialization of system (3.11).

268 The main difference between (3.4) and (3.11) is how the boundary condition is  
 269 implemented. Problem (3.4) enforces the Dirichlet boundary condition in a pointwise  
 270 manner, while (3.11) enforces the Dirichlet boundary condition in a weak sense so  
 271 that pointwise mismatch is allowed.

272 **4. Discretization of the IVPs (3.4) and (3.11) by operator-splitting.** In  
 273 this section, we are going to apply the Lie scheme to the time-discretization of the  
 274 initial value problems (3.4) and (3.11); see [29] for details on the Lie scheme. In  
 275 our splitting strategy, each evolution step is split into several fractional steps so that  
 276 at each fractional step, we only focus on a few operators and update each variable  
 277 implicitly and independently instead of solving a large system including all variables  
 278 simultaneously. Another benefit is that with this strategy,  $\mathbf{p}$  and  $\mathbf{s}$  are updated using  
 279 the already updated  $u$ , which, in general, will improve the convergence behavior of  
 280 the algorithm.

281 In the following, let  $\Delta t (> 0)$  denote a time-discretization step,  $t^n = n\Delta t$ , and  
 282 let  $(u^n, \mathbf{p}^n, \mathbf{s}^n)$  denote an approximation of  $(u, \mathbf{p}, \mathbf{s})$  at  $t = t^n$ .

283 **4.1. Time discretization of the initial value problem (3.4).** The Lie-  
 284 scheme we employ here is a variant of the one we used in [28] to solve the Monge-  
 285 Ampère equation (1.2) completed by a Dirichlet boundary condition. It reads as:

$$286 \quad (4.1) \quad (u^0, \mathbf{p}^0, \mathbf{s}^0) = (u_0, \mathbf{p}_0, \mathbf{s}_0).$$

287 For  $n \geq 0$ ,  $(u^n, \mathbf{p}^n, \mathbf{s}^n) \rightarrow (u^{n+1/2}, \mathbf{p}^{n+1/2}, \mathbf{s}^{n+1/2}) \rightarrow (u^{n+1}, \mathbf{p}^{n+1}, \mathbf{s}^{n+1})$  as follows:

288 The First Fractional Step:

289 Solve

$$290 \quad (4.2) \quad \begin{cases} \frac{\partial u}{\partial t} - \nabla \cdot [(\varepsilon \mathbf{I} + \text{cof}(\mathbf{p}^n)) \nabla u] + 2K(1 + |\mathbf{s}^n|^2)^2 = 0 & \text{in } \Omega \times (t^n, t^{n+1}), \\ u = g & \text{on } \partial\Omega \times (t^n, t^{n+1}), \\ \frac{\partial \mathbf{p}}{\partial t} = \mathbf{0} \text{ in } \Omega \times (t^n, t^{n+1}), \\ \frac{\partial \mathbf{s}}{\partial t} = \mathbf{0} \text{ in } \Omega \times (t^n, t^{n+1}), \\ (u, \mathbf{p}, \mathbf{s})(t^n) = (u^n, \mathbf{p}^n, \mathbf{s}^n), \end{cases}$$

291 and set

292 (4.3)  $u^{n+1/2} = u(t^{n+1}), \quad \mathbf{p}^{n+1/2} = \mathbf{p}(t^{n+1})(= \mathbf{p}^n), \quad \mathbf{s}^{n+1/2} = \mathbf{s}(t^{n+1})(= \mathbf{s}^n).$

293 The Second Fractional Step:

294 Solve

295 (4.4) 
$$\begin{cases} \frac{\partial u}{\partial t} = 0 & \text{in } \Omega \times (t^n, t^{n+1}), \\ \frac{\partial \mathbf{p}}{\partial t} + \gamma_1(\mathbf{p} - \mathbf{D}^2 u^{n+1/2}) = 0 & \text{in } \Omega \times (t^n, t^{n+1}), \\ \frac{\partial \mathbf{s}}{\partial t} + \gamma_2(\mathbf{s} - \nabla u^{n+1/2}) = 0 & \text{in } \Omega \times (t^n, t^{n+1}), \\ (u, \mathbf{p}, \mathbf{s})(t^n) = (u^{n+1/2}, \mathbf{p}^{n+1/2}, \mathbf{s}^{n+1/2}), \end{cases}$$

296 and set

297 (4.5)  $u^{n+1} = u(t^{n+1})(= u^{n+1/2}), \quad \mathbf{p}^{n+1} = P_+[\mathbf{p}(t^{n+1})], \quad \mathbf{s}^{n+1} = \mathbf{s}(t^{n+1}).$

298 In (4.5),  $P_+(\cdot)$  is a (kind of) projection operator which maps the space of the  $2 \times 2$   
299 symmetric matrices onto the closed cone of the  $2 \times 2$  symmetric positive semi-definite  
300 matrices; we will return to operator  $P_+$  in Section 5.6.

We still need to solve the initial value problems that one encounters in (4.2) and (4.4). There is no difficulty with (4.4) since the three initial value problems it contains have closed form solutions, leading to

$$\begin{cases} u(t^{n+1}) = u^{n+1/2}, \\ \mathbf{p}(t^{n+1}) = e^{-\gamma_1 \Delta t} \mathbf{p}^n + (1 - e^{-\gamma_1 \Delta t}) \mathbf{D}^2 u^{n+1}, \\ \mathbf{s}(t^{n+1}) = e^{-\gamma_2 \Delta t} \mathbf{s}^n + (1 - e^{-\gamma_2 \Delta t}) \nabla u^{n+1}. \end{cases}$$

It remains to solve the parabolic problem (4.2); for its solution, we advocate performing just one step of the backward Euler scheme, which enables us to use a relatively large time step while keeping the algorithm stable. We obtain then

$$\begin{cases} \frac{u^{n+1} - u^n}{\Delta t} - \nabla \cdot [(\varepsilon \mathbf{I} + \text{cof}(\mathbf{p}^n)) \nabla u^{n+1}] + 2K(1 + |\mathbf{s}^n|^2)^2 = 0 & \text{in } \Omega, \\ u^{n+1} = g & \text{on } \partial\Omega, \end{cases}$$

301 a (relatively) simple Dirichlet problem for a linear self-adjoint second-order strongly  
302 elliptic operator with variable coefficients, well-suited to finite-element approximations  
303 as we shall see in Section 5.

304 Collecting the above results, we will employ the following time-discretization  
305 scheme to solve the initial value problem (3.4):

306 (4.6)  $(u^0, \mathbf{p}^0, \mathbf{s}^0) = (u_0, \mathbf{p}_0, \mathbf{s}_0).$

307 For  $n \geq 0$ ,  $(u^n, \mathbf{p}^n, \mathbf{s}^n) \rightarrow (u^{n+1}, \mathbf{p}^{n+1}, \mathbf{s}^{n+1})$  as follows:

308 Solve

309 (4.7) 
$$\begin{cases} \frac{u^{n+1} - u^n}{\Delta t} - \nabla \cdot [(\varepsilon \mathbf{I} + \text{cof}(\mathbf{p}^n)) \nabla u^{n+1}] + 2K(1 + |\mathbf{s}^n|^2)^2 = 0 & \text{in } \Omega, \\ u^{n+1} = g & \text{on } \partial\Omega, \end{cases}$$

310 and compute

311 (4.8) 
$$\begin{cases} \mathbf{p}^{n+1} = P_+ [e^{-\gamma_1 \Delta t} \mathbf{p}^n + (1 - e^{-\gamma_1 \Delta t}) \mathbf{D}^2 u^{n+1}], \\ \mathbf{s}^{n+1} = e^{-\gamma_2 \Delta t} \mathbf{s}^n + (1 - e^{-\gamma_2 \Delta t}) \nabla u^{n+1}. \end{cases}$$

312     **4.2. Time discretization of the initial value problem (3.11).** As expected,  
 313     there are many commonalities between the ways we discretize systems (3.4) and (3.11);  
 314     we will take advantage of them. The major difference is that it is much easier to  
 315     operate directly on the variational formulation of the Monge-Ampère part of the  
 316     problem so as to avoid dealing explicitly with the complicated Robin condition we  
 317     visualized in (3.8). Denote the updated boundary condition at  $t^n$  by  $g^n$ . The Lie  
 318     scheme we are going to use reads as:

319     (4.9)      $(u^0, \mathbf{p}^0, \mathbf{s}^0, g^0) = (u_0, \mathbf{p}_0, \mathbf{s}_0, g).$

320     For  $n \geq 0$ ,  $(u^n, \mathbf{p}^n, \mathbf{s}^n, g^n) \rightarrow (u^{n+1/3}, \mathbf{p}^{n+1/3}, \mathbf{s}^{n+1/3}, g^{n+1/3}) \rightarrow$   
 321                     $\rightarrow (u^{n+2/3}, \mathbf{p}^{n+2/3}, \mathbf{s}^{n+2/3}, g^{n+2/3}) \rightarrow (u^{n+1}, \mathbf{p}^{n+1}, \mathbf{s}^{n+1}, g^{n+1}),$

322     where we outline the three fractional steps as the following.

323     The First Fractional Step:

324     Solve

325     (4.10)     
$$\begin{cases} u(t) \in H^1(\Omega), \forall t \in (t^n, t^{n+1}), \\ \int_{\Omega} \frac{\partial u}{\partial t}(t) v dx + \int_{\Omega} \left[ \left( \frac{\varepsilon}{2} \mathbf{I} + \text{cof}(\mathbf{p}(t)) \right) \nabla u(t) \right] \cdot \nabla v dx \\ \quad + 2 \int_{\Omega} K(1 + |\mathbf{s}(t)|^2)^2 dx = 0 \text{ in } \Omega \times (t^n, t^{n+1}), \forall v \in H_0^1(\Omega), \\ u = g^n \text{ on } \partial\Omega \times (t^n, t^{n+1}), \\ \frac{\partial \mathbf{p}}{\partial t} = \mathbf{0} \text{ in } \Omega \times (t^n, t^{n+1}), \\ \frac{\partial \mathbf{s}}{\partial t} = \mathbf{0} \text{ in } \Omega \times (t^n, t^{n+1}), \\ (u, \mathbf{p}, \mathbf{s})(t^n) = (u^n, \mathbf{p}^n, \mathbf{s}^n), \end{cases}$$

326     and set

327     (4.11)      $u^{n+1/3} = u(t^{n+1}), \mathbf{p}^{n+1/3} = \mathbf{p}(t^{n+1}), \mathbf{s}^{n+1/3} = \mathbf{s}(t^{n+1}), g^{n+1/3} = g^n.$

328     The Second Fractional Step:

329     Solve

330     (4.12)     
$$\begin{cases} \frac{\partial u}{\partial t} = 0 \text{ in } \Omega \times (t^n, t^{n+1}), \\ \frac{\partial \mathbf{p}}{\partial t} + \gamma_1(\mathbf{p} - \mathbf{D}^2 u^{n+1/3}) = 0 \quad \text{in } \Omega \times (t^n, t^{n+1}), \\ \frac{\partial \mathbf{s}}{\partial t} + \gamma_2(\mathbf{s} - \nabla u^{n+1/3}) = 0 \quad \text{in } \Omega \times (t^n, t^{n+1}), \\ (u, \mathbf{p}, \mathbf{s})(t^n) = (u^{n+1/3}, \mathbf{p}^{n+1/3}, \mathbf{s}^{n+1/3}), \end{cases}$$

331     and set

332     (4.13)      $u^{n+2/3} = u(t^{n+1}), \mathbf{p}^{n+2/3} = P_+[\mathbf{p}(t^{n+1})], \mathbf{s}^{n+2/3} = \mathbf{s}(t^{n+1}), g^{n+2/3} = g^{n+1/3}.$

333     The Third Fractional Step:

334

335     (4.14)     
$$\begin{cases} u \in H^1(\Omega), \\ \int_{\Omega} \frac{\partial u}{\partial t}(t) v dx + \frac{\varepsilon}{2} \int_{\Omega} \nabla u(t) \cdot \nabla v dx + \kappa \int_{\partial\Omega} (u(t) - g) v d\Gamma = 0, \\ \forall v \in H^1(\Omega), \\ \frac{\partial \mathbf{p}}{\partial t} = \mathbf{0} \text{ in } \Omega \times (t^n, t^{n+1}), \\ \frac{\partial \mathbf{s}}{\partial t} = \mathbf{0} \text{ in } \Omega \times (t^n, t^{n+1}), \\ (u, \mathbf{p}, \mathbf{s})(t^n) = (u^{n+2/3}, \mathbf{p}^{n+2/3}, \mathbf{s}^{n+2/3}), \end{cases}$$

336 and set

337 (4.15)  $u^{n+1} = u(t^{n+1}), \mathbf{p}^{n+1} = P_+ [\mathbf{p}(t^{n+1})], \mathbf{s}^{n+1} = \mathbf{s}(t^{n+1}), g^{n+1} = u^{n+1}|_{\partial\Omega}.$

338 Assuming that one uses just one step of the backward Euler scheme to solve the  
 339 parabolic problem in (4.10) and (4.14), the Lie scheme (4.9)-(4.15) reduces to the  
 340 following variant of scheme (4.6)-(4.8):

341 (4.16)  $(u^0, \mathbf{p}^0, \mathbf{s}^0, g^0) = (u_0, \mathbf{p}_0, \mathbf{s}_0, g).$

342 For  $n \geq 0$ ,  $(u^n, \mathbf{p}^n, \mathbf{s}^n, g^n) \rightarrow (u^{n+1/2}, \mathbf{p}^{n+1}, \mathbf{s}^{n+1}, g^{n+1})$  as follows:

343 Solve

344 (4.17) 
$$\begin{cases} u^{n+1/2} \in H^1(\Omega), \\ \int_{\Omega} \frac{u^{n+1/2} - u^n}{\Delta t} + \int_{\Omega} \left[ \left( \frac{\varepsilon}{2} \mathbf{I} + \text{cof}(\mathbf{p}^n) \right) \nabla u^{n+1/2} \right] \cdot \nabla v dx \\ \quad + 2 \int_{\Omega} K(1 + |\mathbf{s}^n|^2)^2 v dx = 0, \quad \forall v \in H_0^1(\Omega), \\ u^{n+1/2} = g^n \text{ on } \partial\Omega, \end{cases}$$

345 and compute

346 (4.18) 
$$\begin{cases} \mathbf{p}^{n+1} = P_+ [e^{-\gamma_1 \Delta t} \mathbf{p}^n + (1 - e^{-\gamma_1 \Delta t}) \mathbf{D}^2 u^{n+1/2}], \\ \mathbf{s}^{n+1} = e^{-\gamma_2 \Delta t} \mathbf{s}^n + (1 - e^{-\gamma_2 \Delta t}) \nabla u^{n+1/2}, \\ \begin{cases} u \in H^1(\Omega), \\ \int_{\Omega} \frac{u^{n+1} - u^{n+1/2}}{\Delta t} v dx + \frac{\varepsilon}{2} \int_{\Omega} \nabla u^{n+1} \cdot \nabla v dx \\ \quad + \kappa \int_{\partial\Omega} (u^{n+1} - g^n) v d\Gamma = 0, \quad \forall v \in H^1(\Omega), \\ g^{n+1} = u^{n+1}|_{\partial\Omega}. \end{cases} \end{cases}$$

347 **5. Finite elements for the new operator-splitting scheme.** The divergence  
 348 form strongly suggests that we apply a finite-element method to implement (4.7)-(4.8)  
 349 and (4.17)-(4.18). Here we choose a mixed finite-element method: we use the same  
 350 function space to approximate  $u$ ,  $\nabla u$ ,  $\mathbf{D}^2 u$ ,  $\mathbf{s}$ , and  $\mathbf{p}$ . Since we will choose basis  
 351 functions to be piecewise affine functions, the resulting approximations are continuous  
 352 piecewise affine on  $\Omega$ .

353 **5.1. Finite-element spaces.** Let  $\mathcal{T}_h$  be the triangulation of the domain  $\Omega$ , and  
 354 let  $h$  denote the maximum edge length of the triangles in  $\mathcal{T}_h$ . Let  $\Sigma_h = \{Q_j\}_{j=1}^{N_h}$  be  
 355 the collection of vertices in  $\mathcal{T}_h$ , where  $Q_i$  denotes a typical vertex. We define the first  
 356 finite-element space as

357 (5.1)  $V_h = \{v | v \in C^0(\bar{\Omega}), v|_T \in P_1, \forall T \in \mathcal{T}_h\},$

358 where  $P_1$  denotes the space of polynomials with degree no larger than 1.

Accordingly, we associate each vertex  $Q_j$  with a shape function  $w_j$  such that

$$w_j \in V_h, w_j(Q_j) = 1, w_j(Q_k) = 0, \quad \forall k = 1, \dots, N_h, \quad k \neq j,$$

where the support of  $w_j$ , denoted  $\theta_j$ , is the union of triangles that have the same  
 common vertex  $Q_j$ , and we denote the area of  $\theta_j$  by  $|\theta_j|$ . The set  $\mathcal{B} = \{w_j\}_{j=1}^{N_h}$  forms  
 a collection of basis functions of  $V_h$ . In other words, we have

$$v = \sum_{j=1}^{N_h} v(Q_j) w_j, \quad \forall v \in V_h.$$

359 In addition, we define

360 (5.2) 
$$V_{gh} = \{v | v \in V_h, v(Q_j) = g(Q_j), \forall Q_j \in \Sigma_h \cap \partial\Omega\},$$

where  $g$  can be any function which is  $C^0$  on  $\partial\Omega$ . When  $g = 0$ , we have that

$$V_{0h} = V_h \cap H_0^1.$$

361 Meanwhile, we define the following vector-valued spaces

362 
$$\mathbf{R}_h = \{\mathbf{r} | \mathbf{r} \in V_h^{2 \times 1}\},$$
  
363 
$$\mathbf{Q}_h = \{\mathbf{q} | \mathbf{q} \in V_h^{2 \times 2}, \mathbf{q} = \mathbf{q}^T\},$$

364 so that we can use functions in  $\mathbf{R}_h$  to approximate  $\nabla u$  and  $\mathbf{s}$  and use functions in  $\mathbf{Q}_h$   
365 to approximate  $\mathbf{D}^2 u$  and  $\mathbf{p}$ .

366 **5.2. Approximations of the two first-order derivatives of  $u$ .** For any  $v \in$   
367  $V_h$ , we denote the first-order derivative approximation  $\frac{\partial v}{\partial x_i}$  of  $v$  by  $D_{ih}(v)$  for  $i = 1, 2$ ,  
368 and this approximate derivative operator is defined in the following weak sense:

369 (5.3) 
$$\int_{\Omega} D_{ih}(v) w dx = \int_{\Omega} \frac{\partial v}{\partial x_i} w dx, \quad i = 1, 2, \forall w \in H^1(\Omega).$$

370 Since  $\Omega$  is partitioned by the triangulation  $\mathcal{T}_h$ , we restrict the test functions  $w$  to be  
371 in  $V_h$  so that we only need to test the above integral against those basis functions  $w_k$   
372 for  $k = 1, 2, \dots, N_h$ . Since  $w_k$  is only supported on  $\theta_k$ , we have

373 (5.4) 
$$\begin{cases} D_{ih}(v) \in V_h, \quad \forall i = 1, 2, \\ D_{ih}(v)(Q_k) = \frac{3}{|\theta_k|} \int_{\theta_k} \frac{\partial v}{\partial x_i} w_k dx, \quad \forall k = 1, 2, \dots, N_h. \end{cases}$$

374 We remark in passing that on a regular mesh such as the one shown in Figure  
375 1(a), (5.4) recovers the central-difference approximation at an interior node and one-  
376 sided approximation at a boundary node in a finite-difference method based on this  
377 mesh.

378 In some problems,  $\nabla u$  has singularities on  $\Omega$ . One challenging situation is when  
379 the singularities appear on the boundary. The approximation at nodes near the  
380 boundary can blow up, especially when the gradient of the exact solution blows up  
381 at the boundary of a computational domain, such as a semi-sphere. To resolve this  
382 problem, we need to regularize the approximation of  $\nabla u$ . One possible way is to adopt  
383 the idea from [28, 8] which is used to approximate the second-order derivative:

384 (5.5) 
$$\begin{cases} D_{ih}(v) \in H_0^1, \\ \varepsilon_1 \int_{\Omega} \nabla D_{ih} \cdot \nabla w dx + \int_{\Omega} D_{ih}(v) w dx = \int_{\Omega} \frac{\partial v}{\partial x_i} w dx, \quad i = 1, 2, \forall w \in H_0^1(\Omega). \end{cases}$$

The error of the regularized approximation can be larger than that of the direct  
approximation, but it is more robust. Moreover, we have

$$\lim_{\varepsilon_1, h \rightarrow 0} D_{ih}(v) = \frac{\partial v}{\partial x_i} \quad \text{in } L^2(\Omega).$$

385 **5.3. Approximations of second-order derivatives of  $u$ .** The general idea  
 386 to approximate the second-order derivatives is similar to the one used in [22, 12, 28].  
 387 For completeness, we mention the details here.

388 For any  $v \in V_h$ , we denote the approximations of  $\frac{\partial^2 v}{\partial x_i \partial x_j}$  by  $D_{ijh}^2(v)$  for  $i, j = 1, 2$ ,  
 389 so that the approximate operator  $D_{ijh}^2(v)$  of second-order derivatives is defined in the  
 390 following weak sense,

391 (5.6) 
$$\int_{\Omega} D_{ijh}^2(v) w_k dx = \int_{\Omega} \frac{\partial^2 v}{\partial x_i \partial x_j} w_k dx.$$

392 To resolve the right hand side of (5.6), we apply the divergence theorem,

393 (5.7) 
$$\int_{\Omega} \frac{\partial^2 v}{\partial x_i \partial x_j} w dx = \frac{1}{2} \int_{\partial\Omega} \left( \frac{\partial v}{\partial x_i} n_j + \frac{\partial v}{\partial x_j} n_i \right) w d(\partial\Omega) - \frac{1}{2} \int_{\Omega} \left( \frac{\partial v}{\partial x_i} \frac{\partial w}{\partial x_j} + \frac{\partial v}{\partial x_j} \frac{\partial w}{\partial x_i} \right) dx,$$

394 where  $\mathbf{n} = (n_1, n_2)$  is the outward normal direction along  $\partial\Omega$ . The above approximation  
 395 is accurate at interior nodes, but the approximation error is large at nodes on  
 396 the boundary. For example, consider the approximate derivative operator  $D_{11h}^2$  on  
 397 a regular mesh of the unit square; after some derivation, we can show that there is  
 398 always one node at one of the corners of the unit square such that  $D_{11h}^2(v) = 0$  at  
 399 that node, no matter what form  $v$  takes.

400 To deal with this issue, we treat interior nodes and boundary nodes separately. Let  
 401  $\Sigma_{0h} = \{Q_k\}_{k=1}^{N_0}$  denote the set of interior nodes in  $\Omega$ , where we assume that the first  
 402  $N_0$  nodes of  $\Sigma_h$  are in the interior of  $\Omega$ . It follows that we have  $\Sigma_h \cap \partial\Omega = \{Q_k\}_{k=N_0+1}^{N_h}$ .  
 403 For  $k = 1, 2, \dots, N_0$ , the approximation of (5.6)-(5.7) reduces to

404 (5.8) 
$$\int_{\Omega} D_{ijh}^2(v) w_k dx = -\frac{1}{2} \int_{\Omega} \left( \frac{\partial v}{\partial x_i} \frac{\partial w_k}{\partial x_j} + \frac{\partial v}{\partial x_j} \frac{\partial w_k}{\partial x_i} \right) dx.$$

405 To treat nodes on the boundary, the work in [8] used the zero Dirichlet boundary  
 406 condition for the operator  $D_{ijh}^2$ ,  $i, j = 1, 2$ , though the boundary value is not needed  
 407 in the resulting algorithm. In comparison with the numerical method in [8], ours are  
 408 different in that the boundary value of  $D_{ijh}^2$  is crucial for our splitting algorithm.  
 409 Specifically, in (4.7)-(4.8) we need boundary values to update  $\mathbf{p}$  which is in turn used  
 410 to compute the divergence operator and to update  $u$ . Therefore, we need a better  
 411 treatment of the boundary nodes.

412 Here we adopt a strategy from [28, 38] to treat boundary nodes by committing a  
 413 “variational crime”. First, we impose the zero Neumann boundary condition

414 (5.9) 
$$\frac{\partial D_{ijh}^2(v)}{\partial \mathbf{n}} = 0.$$

415 Multiplying (5.9) by  $w_k$  for  $k = N_0 + 1, \dots, N_h$  and integrating along  $\partial\Omega$ , we get

416 
$$0 = \int_{\partial\Omega} \frac{\partial D_{ijh}^2(v)}{\partial \mathbf{n}} w_k d(\partial\Omega) = \int_{\Omega} \nabla \cdot (\nabla D_{ijh}^2(v) w_k) dx$$
  
 417 (5.10) 
$$= \int_{\Omega} \nabla^2 D_{ijh}^2(v) w_k dx + \int_{\Omega} \nabla D_{ijh}^2(v) \cdot \nabla w_k dx.$$

418 If  $D_{ijh}^2(v)$  is harmonic, implying that  $\nabla^2 D_{ijh}^2(v) = 0$ , then we have

419 (5.11) 
$$\int_{\Omega} \nabla D_{ijh}^2(v) \cdot \nabla w_k dx = 0.$$

In our algorithm, although  $D_{ijh}^2$  is only piecewise harmonic, we still use (5.11) to update boundary values, which is the so-called variational crime. In either approximation (5.6)-(5.7) or approximation (5.8) and (5.11), since  $w_k$  is only supported on  $\theta_k$ , the integration domain can be replaced by  $\theta_k$  if the test function is  $w_k$ . Under certain conditions, a rough derivation shows that the variational crime introduces an error to (5.10) of  $O(h)$ . Since  $D_{ijh}^2(v) \in V_h$ ,  $\nabla D_{ijh}^2(v)$  is piecewise constant over  $\Omega$ . For any  $T \in \mathcal{T}_h$ , let  $\nu$  be one of its edges. Along  $\nu$ ,  $\nabla^2 D_{ijh}^2(v)$  is a Dirac- $\delta$  function multiplied by a factor (the difference of the values of  $\nabla D_{ijh}^2(v)$  over the two triangles having  $\nu$  as the common boundary). In the interior of  $T$ ,  $\nabla^2 D_{ijh}^2(v)$  is 0. Thus

$$\int_{\Omega} \nabla^2 D_{ijh}^2(v) w_k dx = \sum_{T \in \mathcal{T}_h} \int_{\nu \in \partial T} \nabla^2 D_{ijh}^2(v) w_k dx = O(h)$$

420 if  $\nabla D_{ijh}^2(v)$  is bounded by a constant.

421 In our numerical experiments, with the regularization mechanism introduced below,  
422 the accuracy by (5.8) and (5.11) is similar to that by (5.6)-(5.7), but (5.8) and  
423 (5.11) make the algorithm more robust. It is worth mentioning that as implemented  
424 in [28] both approximations work for two-dimensional Monge-Ampère equations; how-  
425 ever, as shown in [38] only the approximation based on the variational crime works  
426 for three-dimensional Monge-Ampère equations.

427 As reported in [8, 28, 38], if we directly use the above approximations, the perfor-  
428 mance of our algorithm depends on triangulations; in the worst case, on a symmetric  
429 mesh as shown in Figure 1(b), our algorithm does not converge. To obtain an algo-  
430 rithm which is robust for all kinds of meshes, we need to regularize the problem by  
431 adding some viscosity to our formulation of second-order derivatives.

432 As a first approach of regularization, we incorporate a local regularization term  
433 into the weak definition of second-order derivatives at interior nodes:

$$434 \quad (5.12) \quad \begin{cases} \forall i, j = 1, 2, \forall v \in V_h, D_{ijh}^2(v) \in V_h \text{ and} \\ C \sum_{T \in \mathcal{T}_h^k} |T| \int_T \nabla D_{ijh}^2(v) \cdot \nabla w_k dx + \int_{\theta_k} D_{ijh}^2(v) w_k dx \\ \quad = -\frac{1}{2} \int_{\theta_k} \left[ \frac{\partial v}{\partial x_i} \frac{\partial w_k}{\partial x_j} + \frac{\partial v}{\partial x_j} \frac{\partial w_k}{\partial x_i} \right] dx, \forall k = 1, \dots, N_{0h}, \\ \int_{\theta_k} \nabla D_{ijh}^2(v) \cdot \nabla w_k dx = 0, \forall k = N_{0h} + 1, \dots, N_h, \end{cases}$$

435 where  $C$  is a positive constant of order 1, and  $\mathcal{T}_h^k$  is the set of all triangles with the  
436 common vertex  $Q_k$ .

437 If all triangles in  $\mathcal{T}_h$  are of a similar size, (5.12) can be slightly simplified to be

$$438 \quad (5.13) \quad \begin{cases} \forall i, j = 1, 2, \forall v \in V_h, D_{ijh}^2(v) \in V_h \text{ and} \\ \varepsilon_1 \int_{\theta_k} \nabla D_{ijh}^2(v) \cdot \nabla w_k dx + \int_{\theta_k} D_{ijh}^2(v) w_k dx \\ \quad = -\frac{1}{2} \int_{\theta_k} \left[ \frac{\partial v}{\partial x_i} \frac{\partial w_k}{\partial x_j} + \frac{\partial v}{\partial x_j} \frac{\partial w_k}{\partial x_i} \right] dx, \forall k = 1, \dots, N_{0h}, \\ \int_{\theta_k} \nabla D_{ijh}^2(v) \cdot \nabla w_k dx = 0, \forall k = N_{0h} + 1, \dots, N_h, \end{cases}$$

439 where  $\varepsilon_1$  is of order  $O(h^2)$ .

440 As a second approach of regularization, we incorporate a double-regularization  
441 mechanism into our weak formulation of second-order derivatives. Assuming that  
442  $\psi \in H^2$ , we consider the following linear elliptic variational problem,

(5.14)

$$443 \quad \begin{cases} p_{ij}^\varepsilon \in H_0^1(\Omega), \\ \varepsilon_1 \int_{\Omega} \nabla p_{ij}^\varepsilon \cdot \nabla \phi dx + \int_{\Omega} p_{ij}^\varepsilon \phi dx = -\frac{1}{2} \int_{\Omega} \left[ \frac{\partial \psi}{\partial x_i} \frac{\partial \phi}{\partial x_j} + \frac{\partial \psi}{\partial x_j} \frac{\partial \phi}{\partial x_i} \right] dx, \forall \phi \in H_0^1(\Omega), \end{cases}$$

444 which yields the following relations in the weak sense

445 (5.15) 
$$\lim_{\varepsilon_1 \rightarrow 0} p_{ij}^\varepsilon = \frac{\partial^2 \psi}{\partial x_i \partial x_j} \quad \text{in } L^2(\Omega),$$

446 and

447 (5.16) 
$$\begin{cases} -\varepsilon_1 \nabla^2 p_{ij}^\varepsilon + p_{ij}^\varepsilon = \frac{\partial^2 \psi}{\partial x_i \partial x_j} & \text{in } \Omega, \\ p_{ij}^\varepsilon = 0 & \text{on } \partial\Omega. \end{cases}$$

448 Since, as reported in [28], this approximation is not effective in treating the zero-  
449 Dirichlet boundary condition, we apply the following correction step,

450 (5.17) 
$$\begin{cases} -\varepsilon_1 \nabla^2 \tilde{p}_{ij}^\varepsilon + \tilde{p}_{ij}^\varepsilon = p_{ij}^\varepsilon & \text{in } \Omega, \\ \frac{\partial \tilde{p}_{ij}^\varepsilon}{\partial \mathbf{n}} = 0 & \text{on } \partial\Omega, \end{cases}$$

451 whose variational formulation reads as

452 (5.18) 
$$\begin{cases} \tilde{p}_{ij}^\varepsilon \in H^1(\Omega), \\ \varepsilon_1 \int_{\Omega} \nabla \tilde{p}_{ij}^\varepsilon \cdot \nabla \phi dx + \int_{\Omega} \tilde{p}_{ij}^\varepsilon \phi dx = \int_{\Omega} p_{ij}^\varepsilon \phi dx, \quad \forall \phi \in H^1(\Omega). \end{cases}$$

453 It follows that  $\tilde{p}_{ij}^\varepsilon$  verifies  $\lim_{\varepsilon \rightarrow 0} \tilde{p}_{ij}^\varepsilon = \frac{\partial^2 \psi}{\partial x_i \partial x_j}$  in  $L^2(\Omega)$ , and  $\tilde{p}_{ij}^\varepsilon \in H^4(\Omega)$ .

454 Consequently, the discrete analogue  $D_{ijh}^2(v)$  of  $\frac{\partial^2 v}{\partial x_i \partial x_j}$  ( $1 \leq i, j \leq 2$ ) can be com-  
455 puted in the following way:

456 Solve:

(5.19) 
$$\begin{cases} p_{ij} \in V_{0h}, \\ C \sum_{T \in \mathcal{T}_h^k} |T| \int_T \nabla p_{ij} \cdot \nabla w_k dx + \frac{|\theta_k|}{3} p_{ij}(Q_k) = -\frac{1}{2} \int_{\theta_k} \left[ \frac{\partial v}{\partial x_i} \frac{\partial w_k}{\partial x_j} + \frac{\partial v}{\partial x_j} \frac{\partial w_k}{\partial x_i} \right] dx, \\ \forall k = 1, \dots, N_{0h}, \end{cases}$$

458 and then

459 (5.20) 
$$\begin{cases} D_{ijh}^2(v) \in V_h, \\ C \sum_{T \in \mathcal{T}_h^k} |T| \int_T \nabla D_{ijh}^2(v) \cdot \nabla w_k dx + \frac{|\theta_k|}{3} D_{ijh}^2(v)(Q_k) = \frac{|\theta_k|}{3} p_{ij}(Q_k), \\ \forall k = 1, \dots, N_h, \end{cases}$$

460 where  $C$  is a constant of order 1. Similar to the first approach of regularization, if all  
461 triangles in  $\mathcal{T}_h$  are of a similar size, we can replace  $C \sum_{T \in \mathcal{T}_h^k} |T|$  in (5.19) and (5.20)  
462 by  $\epsilon_1$  which is of order  $O(h^2)$ .

463 **5.4. Implementation of scheme (4.6)-(4.8).** We give a fully discretized ana-  
464 logue of scheme (4.6)-(4.8) as follows.

465 Initialize

466 (5.21) 
$$u^0 = u_0 \in V_h, \mathbf{p}^0 = \mathbf{p}_0 \in \mathbf{Q}_h, \mathbf{s}^0 = \mathbf{s}_0 \in \mathbf{R}_h.$$

467 For  $n \geq 0$ , proceed  $\{u^n, \mathbf{p}^n, \mathbf{s}^n\} \rightarrow \{u^{n+1}, \mathbf{p}^{n+1}, \mathbf{s}^{n+1}\}$  as the following.

468 Solve

469 (5.22) 
$$\begin{cases} u^{n+1} \in V_{gh}, \\ \int_{\Omega} u^{n+1} v dx + \Delta t \int_{\Omega} (\varepsilon \mathbf{I} + \text{cof}(\mathbf{p}^n)) \nabla u^{n+1} \cdot \nabla v dx \\ \quad = \int_{\Omega} u^n v dx - 2\Delta t K \int_{\Omega} (1 + |\mathbf{s}^n|^2)^2 dx, \quad \forall v \in V_{0h}, \end{cases}$$

470 and compute  $\mathbf{p}^{n+1}$  and  $\mathbf{s}^{n+1}$  via

(5.23)

$$471 \quad \begin{cases} \forall k = 1, \dots, N_h, \\ \alpha = e^{-\gamma_1 \Delta t}, \\ \mathbf{p}^{n+\frac{1}{2}}(Q_k) = \alpha \mathbf{p}^n(Q_k) + (1 - \alpha) \begin{pmatrix} D_{11h}^2(u^{n+1})(Q_k) & D_{12h}^2(u^{n+1})(Q_k) \\ D_{12h}^2(u^{n+1})(Q_k) & D_{22h}^2(u^{n+1})(Q_k) \end{pmatrix}, \\ \mathbf{p}^{n+1}(Q_k) = P_+ [\mathbf{p}^{n+1/2}(Q_k)]. \end{cases}$$

472 and

$$473 \quad (5.24) \quad \begin{cases} \forall k = 1, \dots, N_h, \\ \mathbf{s}^{n+1}(Q_k) = e^{-\gamma_2 \Delta t} \mathbf{s}^n(Q_k) + (1 - e^{-\gamma_2 \Delta t}) \begin{pmatrix} D_{1h}(u^{n+1})(Q_k) \\ D_{2h}(u^{n+1})(Q_k) \end{pmatrix}. \end{cases}$$

474 Here, all integrations in (5.22) are computed by the trapezoidal rule. In (5.23) and  
475 (5.24),  $D_{ih}^1$  for  $i = 1, 2$  are computed using (5.5) or (5.3);  $D_{ijh}^2(u^{n+1})$  for  $i, j = 1, 2$   
476 are computed by approximation (5.12) or (5.19)-(5.20).

477 **5.5. Implementation of scheme (4.16)-(4.18).** The discretized analogue of  
478 scheme (4.6)-(4.8) can be written as:

479 Initialize

$$480 \quad (5.25) \quad u^0 = u_0 \in V_h, \mathbf{p}^0 = \mathbf{p}_0 \in \mathbf{Q}_h, \mathbf{s}^0 = \mathbf{s}_0 \in \mathbf{R}_h, g^0 = g.$$

481 For  $n \geq 0$ , proceed  $\{u^n, \mathbf{p}^n, \mathbf{s}^n\} \rightarrow \{u^{n+1}, \mathbf{p}^{n+1}, \mathbf{s}^{n+1}\}$  as the following.  
482 Solve

$$483 \quad (5.26) \quad \begin{cases} u^{n+1/2} \in V_{g^n h}, \\ \int_{\Omega} u^{n+1/2} v dx + \Delta t \int_{\Omega} (\varepsilon \mathbf{I} + \text{cof}(\mathbf{p}^n)) \nabla u^{n+1/2} \cdot \nabla v dx \\ \quad = \int_{\Omega} u^n v dx - 2\Delta t K \int_{\Omega} (1 + |\mathbf{s}^n|^2)^2 dx, \forall v \in V_{g^n h}. \end{cases}$$

484 Compute  $\mathbf{p}^{n+1}$  and  $\mathbf{s}^{n+1}$  via

(5.27)

$$485 \quad \begin{cases} \forall k = 1, \dots, N_h, \\ \alpha = e^{-\gamma_1 \Delta t}, \\ \mathbf{p}^{n+\frac{1}{2}}(Q_k) = \alpha \mathbf{p}^n(Q_k) + (1 - \alpha) \begin{pmatrix} D_{11h}^2(u^{n+1/2})(Q_k) & D_{12h}^2(u^{n+1/2})(Q_k) \\ D_{12h}^2(u^{n+1/2})(Q_k) & D_{22h}^2(u^{n+1/2})(Q_k) \end{pmatrix}, \\ \mathbf{p}^{n+1}(Q_k) = P_+ [\mathbf{p}^{n+1/2}(Q_k)]. \end{cases}$$

486 and

$$487 \quad (5.28) \quad \begin{cases} \forall k = 1, \dots, N_h, \\ \mathbf{s}^{n+1}(Q_k) = e^{-\gamma_2 \Delta t} \mathbf{s}^n(Q_k) + (1 - e^{-\gamma_2 \Delta t}) \begin{pmatrix} D_{1h}(u^{n+1/2})(Q_k) \\ D_{2h}(u^{n+1/2})(Q_k) \end{pmatrix}. \end{cases}$$

488 Compute

$$489 \quad (5.29) \quad \begin{cases} u^{n+1} \in V_h, \\ \int_{\Omega} u^{n+1} v dx + \Delta t \varepsilon \int_{\Omega} \nabla u^{n+1} \cdot \nabla v dx + \Delta t \int_{\partial\Omega} u^{n+1} v dx \\ \quad = \int_{\Omega} u^{n+1/2} v dx + \Delta t \varepsilon \int_{\partial\Omega} g v dx, \forall v \in V_h. \end{cases}$$

490 and update

491 (5.30) 
$$g^{n+1} = u^{n+1}|_{\partial\Omega}.$$

492 All integrations in (5.26) and (5.29) are computed by the trapezoidal rule. In (5.27)  
493 and (5.28),  $D_{ih}^1$  for  $i = 1, 2$  are computed using (5.5) or (5.3);  $D_{ijh}^2(u^{n+1})$  for  $i, j = 1, 2$   
494 are computed by approximation (5.12) or (5.19)-(5.20).

495 **5.6. The projection operator  $P_+(\cdot)$ .** Since we want to find a convex solution  
496  $u$ , we need to have some mechanism to enforce convexity in our algorithm. There are  
497 many possible approaches to handle the issue.

498 One particular approach that we discuss here is to modify one of the finite-element  
499 components,  $\mathbf{p}$ , after each iteration so that the modified  $\mathbf{p}$  satisfies some convexity-  
500 related properties. Since the Hessian matrix of a convex function is semi-positive  
501 definite and we expect  $\mathbf{p}$  to converge to the Hessian matrix of the exact solution  $u^*$   
502 which is convex, it is reasonable to enforce  $\mathbf{p}$  to be semi-positive definite; therefore, we  
503 introduce a spectral projection operator to achieve this, and  $P_+(\cdot)$  is such a projector  
504 in our algorithm.

Let  $\mathbf{A}$  be a symmetric  $2 \times 2$  matrix. Assume that  $\mathbf{A}$  has a spectral decomposition,  

$$\mathbf{A} = \mathbf{S}\mathbf{\Lambda}\mathbf{S}^{-1}$$
, where the columns of  $\mathbf{S}$  are the eigenvectors of  $\mathbf{A}$  and  $\mathbf{\Lambda} = \begin{pmatrix} \lambda_1 & 0 \\ 0 & \lambda_2 \end{pmatrix}$ .

We define the spectral projector operator  $P_+(\cdot)$  as

$$P_+(\mathbf{A}) = \mathbf{S} \begin{pmatrix} \lambda_1^+ & 0 \\ 0 & \lambda_2^+ \end{pmatrix} \mathbf{S}^{-1},$$

505 where  $\lambda_i^+ = \max\{\lambda_i, 0\}$  for  $i = 1, 2$ . The effect of  $P_+(\mathbf{A})$  is to project  $\mathbf{A}$  onto the cone  
506 consisting of semi-positive definite matrices. This projection during each iteration  
507 makes equation (4.7) an elliptic PDE of  $u$ .

508 Another possible approach is to choose a convex initial condition which will be  
509 discussed in the next section.

510 **6. Initialization.**

511 **6.1. Initial condition for scheme (4.6)-(4.8).** To initialize  $u_0$  and  $\mathbf{p}_0$  for  
512 scheme (4.6)-(4.8), we solve the standard Monge-Ampère equation

513 (6.1) 
$$\begin{cases} \det(\mathbf{D}^2 u_0) = K, \\ u_0 = g \text{ on } \partial\Omega. \end{cases}$$

514 We will deal with (6.1) by adopting the method in [28], which solves the following  
515 initial value problem to steady state,

516 (6.2) 
$$\begin{cases} \begin{cases} \frac{\partial u}{\partial t} - \nabla \cdot ((\varepsilon \mathbf{I} + \text{cof}(\mathbf{p})) \nabla u) + 2K = 0, \\ u = g \text{ on } \partial\Omega, \\ \frac{\partial \mathbf{p}}{\partial t} + \gamma(\mathbf{p} - \mathbf{D}^2 u) = \mathbf{0}. \end{cases} \end{cases}$$

517 Let  $\{u_*, \mathbf{p}_*\}$  be the steady state of (6.2). Accordingly, we set  $u_0 = u_*$ ,  $\mathbf{p}_0 = \mathbf{D}^2 u_*$   
518 and  $\mathbf{s} = \mathbf{D}u_*$  as the initial condition for our scheme (4.6)-(4.8). Therefore, our  
519 algorithm can be summarized as a two-stage method:

**Stage 1**

In the algorithm in [28], set  $\varepsilon = \varepsilon_1 = h^2$  and  $dt = 2h^2$ . Solve (6.2) until  
520  $\|u^{n+1} - u^n\|_2 < tol$  to get  $u_0$ . Compute  $\mathbf{p}_0 = \mathbf{D}^2 u_0$  and  $\mathbf{s}_0 = \mathbf{D}u_0$ .

**Stage 2**

With the initial condition  $u_0$ ,  $\mathbf{p}_0$ , and  $\mathbf{s}_0$ , solve (4.6)-(4.8) to steady state.

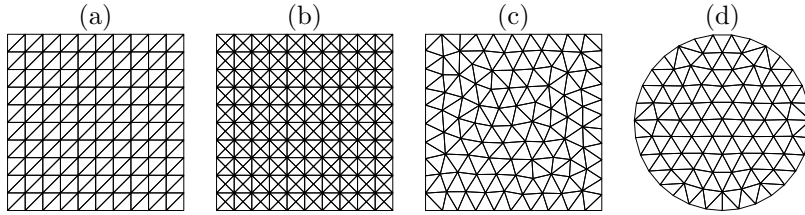


FIG. 1. Four meshes for two different domains used in our numerical experiments. (a) A regular mesh on a square. (b) A (highly) symmetric mesh on a square. (c) An anisotropic unstructured mesh on a square. (d) An anisotropic unstructured mesh on a half-unit disk.

521     **6.2. Initial condition for scheme (4.16)-(4.18).** When we use scheme (4.16)-  
 522     (4.18), the boundary value of the computed solution does not satisfy the given bound-  
 523     ary condition, so the initial condition used for scheme (4.6)-(4.8) may not help. To  
 524     initialize scheme (4.16)-(4.18), we use the initial condition used to solve (6.2) in [28]:

$$525 \quad (6.3) \quad \begin{cases} \nabla^2 u_0 = 2\lambda\sqrt{K}, \\ u_0|_{\partial\Omega} = g, \end{cases}$$

526 where  $\lambda$  ( $> 0$ ) is of order  $O(1)$ .

527     **7. Numerical experiments.** In this section, we carry out a variety of numerical  
 528     experiments in different settings to demonstrate the performance of scheme (4.6)-(4.8)  
 529     and scheme (4.16)-(4.18). Four different meshes as shown in Figure 1 will be used  
 530     in our experiments: (a) regular meshes on a unit square, (b) symmetric meshes on a  
 531     unit square, (c) unstructured meshes on a unit square, and (d) unstructured meshes  
 532     on a half-unit disk. In all of our experiments, in Stage 1 of our algorithm, we use the  
 533     method in [28] to initialize the iteration of our algorithm, where we use  $tol = h^2$ .

534     There are several parameters in our algorithm:  $\gamma_1$  and  $\gamma_2$  (defined in Section  
 535     3.2),  $\varepsilon$  (regularization parameter in the PDE (3.3)),  $\varepsilon_1$  (regularization parameter in  
 536     the first order and second order derivative approximation in Section 5.2 and 5.3),  
 537     and time step  $\Delta t$ . In general, when a smooth solution exists, our algorithm is not  
 538     sensitive to the choice of parameters. Setting  $\varepsilon$  and  $\varepsilon_1$  in the order of  $h^2$  and  $\beta_1$   
 539     and  $\beta_2$  (in the formulas of  $\gamma_1$  and  $\gamma_2$ ) of  $O(1)$  makes the algorithm stable. The time  
 540     step  $\Delta t$  determines how fast our algorithm converges. Our algorithm converges as  
 541     long as  $\Delta t$  is small enough and other parameters are set as mentioned above. A  
 542     large  $\Delta t$  will make our algorithm converge faster, but it may destroy the stability. In  
 543     our experiments, setting  $\Delta t$  in the order of  $h^2$  makes our algorithm yield reasonable  
 544     results. For some problems with singular solutions or derivatives blowing up along  
 545     boundaries, we will take both  $\varepsilon$  and  $\varepsilon_1$  to be a larger value and take  $\Delta t$  to be a smaller  
 546     value in order to stabilize the algorithm.

547     Without specification, we choose  $\Delta t = 2h^2$  and  $\varepsilon = \varepsilon_1 = h^2$  in both Stage 1 and  
 548     2 of our algorithm. For examples with compatible boundary condition, scheme (4.6)-  
 549     (4.8) is used. For examples with incompatible boundary condition, scheme (4.16)-  
 550     (4.18) is used. We also compare the numerical solutions by both schemes on some  
 551     examples. Without specification, stopping criterion  $\|u^{n+1} - u^n\|_2 < 10^{-6}$  and scheme  
 552     (4.6)-(4.8) are used. This stopping criterion is selected so that our algorithm converges  
 553     on all meshes. This criterion may be demanding for some coarse meshes, as many  
 554     iterations are not necessary. Nevertheless, our current setting does not affect the  
 555     demonstration of the performance of our proposed algorithms. A more practical way

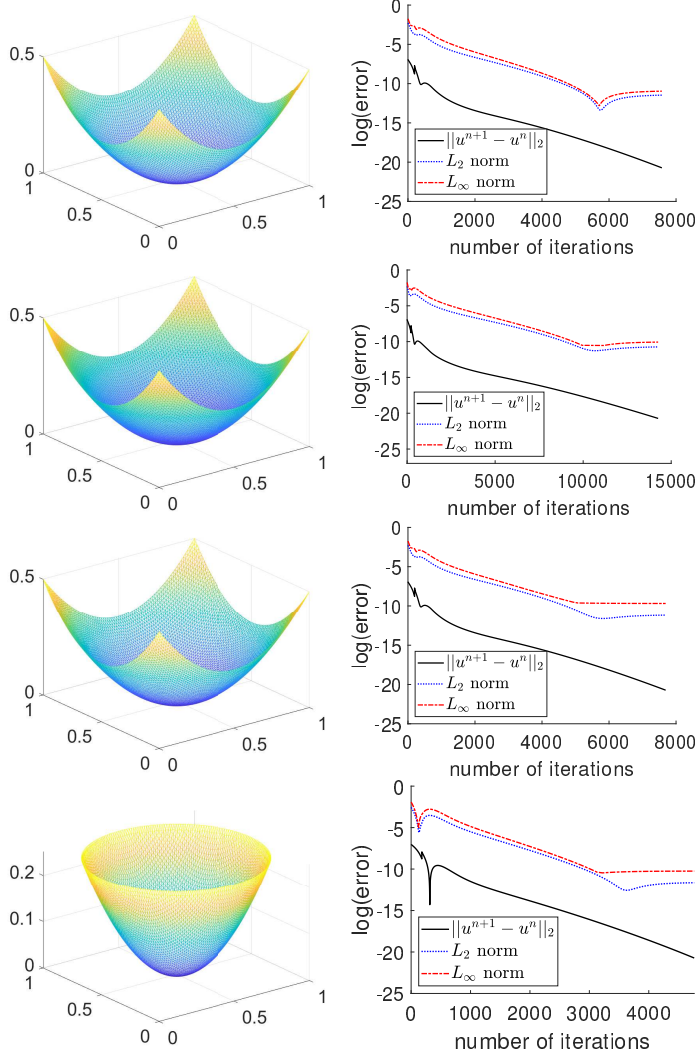


FIG. 2. (Test problem (7.1) with  $\alpha = 1$ . Scheme (4.6)-(4.8).) Graphs of the computed solutions and the related convergence history. Roe 1: Regular triangulation of the unit square. Row 2: Symmetric triangulation of the unit square. Row 3: Unstructured anisotropic triangulation of the unit square. Row 4: Unstructured anisotropic triangulation of a half-unit disk. The second-order derivatives are approximated by (5.13).

556 is to set the stopping criterion depending on  $h$ . Additional numerical results are  
 557 presented in the supplementary materials.

558 **7.1. Example 1.** For the first example, we choose the exact solution  $u^*$  as a  
 559 quadratic function,

560 (7.1) 
$$u^* = \alpha (x_1 - 0.5)^2 + (x_2 - 0.5)^2 / \alpha,$$

561 so that the Gauss curvature  $K = \frac{4}{1+4\alpha(x_1-0.5)^2+\frac{4}{\alpha}(x_2-0.5)^2}$  and the boundary condition  
 562  $g = u^*|_{\partial\Omega}$ , where  $\alpha$  is a positive constant.

563 Since the solution of this example is smooth, we use (5.4) to approximate the

	$h$	Iterations	$\ u^{n+1} - u^n\ $	$L_2$ norm	rate	$L_\infty$ norm	rate
(a)	1/10	193	$9.88 \times 10^{-10}$	$6.06 \times 10^{-4}$		$9.86 \times 10^{-4}$	
	1/20	606	$9.81 \times 10^{-10}$	$1.66 \times 10^{-4}$	1.87	$2.73 \times 10^{-4}$	1.85
	1/40	2064	$9.96 \times 10^{-10}$	$4.34 \times 10^{-5}$	1.94	$7.11 \times 10^{-5}$	1.94
	1/80	7577	$9.99 \times 10^{-10}$	$1.05 \times 10^{-5}$	2.05	$1.73 \times 10^{-5}$	2.04
(b)	$h$	Iterations	$\ u^{n+1} - u^n\ $	$L_2$ norm	rate	$L_\infty$ norm	rate
	1/10	305	$9.99 \times 10^{-10}$	$1.37 \times 10^{-3}$		$2.64 \times 10^{-3}$	
	1/20	1021	$9.99 \times 10^{-10}$	$3.53 \times 10^{-4}$	1.96	$6.88 \times 10^{-4}$	1.94
	1/40	3961	$9.99 \times 10^{-10}$	$8.98 \times 10^{-5}$	1.97	$1.75 \times 10^{-4}$	1.98
(c)	1/80	14259	$9.99 \times 10^{-10}$	$2.16 \times 10^{-5}$	2.06	$4.24 \times 10^{-5}$	2.05
	$h$	Iterations	$\ u^{n+1} - u^n\ $	$L_2$ norm	rate	$L_\infty$ norm	rate
	1/10	180	$9.38 \times 10^{-10}$	$5.70 \times 10^{-4}$		$2.04 \times 10^{-3}$	
	1/20	591	$9.80 \times 10^{-10}$	$1.90 \times 10^{-4}$	1.59	$5.99 \times 10^{-4}$	1.77
(d)	1/40	2080	$9.97 \times 10^{-10}$	$5.27 \times 10^{-5}$	1.85	$1.57 \times 10^{-4}$	1.93
	1/80	7690	$9.99 \times 10^{-10}$	$1.42 \times 10^{-5}$	1.89	$6.22 \times 10^{-5}$	1.34
	1/10	111	$8.49 \times 10^{-10}$	$6.10 \times 10^{-4}$		$1.20 \times 10^{-3}$	
	1/20	374	$9.97 \times 10^{-10}$	$1.65 \times 10^{-4}$	1.89	$4.55 \times 10^{-4}$	1.40
	1/40	1221	$9.93 \times 10^{-10}$	$3.61 \times 10^{-5}$	2.20	$1.03 \times 10^{-4}$	2.14
	1/80	4765	$9.97 \times 10^{-10}$	$8.73 \times 10^{-6}$	2.05	$3.54 \times 10^{-5}$	1.54

TABLE 1

(Test problem (7.1) with  $\alpha = 1$ . Scheme (4.6)-(4.8).) Numbers of iterations necessary for convergence, approximation errors and accuracy orders. (a) Regular triangulation of the unit square. (b) Symmetric triangulation of the unit square. (c) Unstructured anisotropic triangulation of the unit square. (d) Unstructured anisotropic triangulation of the half-unit disk. The second-order derivatives are approximated by (5.13).

	$h$	Iterations	$\ u^{n+1} - u^n\ $	$L_2$ norm	rate	$L_\infty$ norm	rate
(a)	1/10	266	$9.50 \times 10^{-8}$	$1.01 \times 10^{-1}$		$1.22 \times 10^{-1}$	
	1/20	512	$9.87 \times 10^{-8}$	$4.02 \times 10^{-2}$	1.33	$4.63 \times 10^{-2}$	1.40
	1/40	1432	$9.99 \times 10^{-8}$	$1.82 \times 10^{-2}$	1.14	$2.13 \times 10^{-2}$	1.12
	1/80	4529	$9.99 \times 10^{-8}$	$8.73 \times 10^{-3}$	1.06	$1.03 \times 10^{-2}$	1.05
(b)	$h$	Iterations	$\ u^{n+1} - u^n\ $	$L_2$ norm	rate	$L_\infty$ norm	rate
	1/10	471	$9.57 \times 10^{-8}$	$8.24 \times 10^{-2}$		$9.74 \times 10^{-2}$	
	1/20	782	$9.95 \times 10^{-8}$	$3.46 \times 10^{-2}$	1.25	$3.97 \times 10^{-2}$	1.29
	1/40	2581	$9.99 \times 10^{-8}$	$1.60 \times 10^{-2}$	1.11	$1.80 \times 10^{-2}$	1.14
	1/80	7690	$9.99 \times 10^{-8}$	$7.78 \times 10^{-3}$	1.04	$8.56 \times 10^{-3}$	1.07

TABLE 2

(Test problem (7.1) with  $\alpha = 1$ . Scheme (4.6)-(4.8).) Numbers of iterations necessary for convergence, approximation errors, and accuracy orders. (a) Regular triangulation of the unit square. (b) Symmetric triangulation of the unit square. The second-order derivatives are approximated by (5.19)-(5.20).

564 first-order derivatives. In the first test, we choose  $\alpha = 1$  so that  $u^*$  represents a  
565 family of con-centric circles which vary isotropically.

566 With the second-order derivatives approximated by (5.13) and scheme (4.6)-(4.8),  
567 the graphs and convergence histories of numerical solutions on different meshes are

$h$	Iterations	$\ u^{n+1} - u^n\ $	$L_2$ norm	rate	$L_\infty$ norm	rate
1/10	198	$9.78 \times 10^{-10}$	$1.88 \times 10^{-3}$		$2.75 \times 10^{-3}$	
1/20	604	$9.80 \times 10^{-10}$	$3.72 \times 10^{-4}$	2.34	$5.91 \times 10^{-4}$	2.22
1/40	2057	$9.92 \times 10^{-10}$	$8.86 \times 10^{-5}$	2.07	$1.44 \times 10^{-4}$	2.04
1/80	7566	$9.99 \times 10^{-10}$	$2.14 \times 10^{-5}$	2.05	$3.53 \times 10^{-5}$	2.03

TABLE 3

(Test problem (7.1) with  $\alpha = 1$ . Scheme (4.16)-(4.18)) Numbers of iterations necessary for convergence, approximation errors, and accuracy orders. The second-order derivatives are approximated by (5.13).

$h$	Iterations	$\ u^{n+1} - u^n\ $	$L_2$ norm	rate	$L_\infty$ norm	rate
1/10	309	$9.67 \times 10^{-10}$	$5.01 \times 10^{-4}$		$8.07 \times 10^{-4}$	
1/20	938	$9.93 \times 10^{-10}$	$1.32 \times 10^{-4}$	1.92	$2.12 \times 10^{-4}$	1.93
1/40	2982	$9.97 \times 10^{-10}$	$3.38 \times 10^{-5}$	2.01	$5.39 \times 10^{-5}$	1.98
1/80	14565	$9.99 \times 10^{-11}$	$8.51 \times 10^{-6}$	1.99	$1.36 \times 10^{-5}$	1.99

TABLE 4

(Test problem (7.1) with  $\alpha = 2$ . Scheme (4.6)-(4.8).) Numbers of iterations necessary for convergence, approximation errors, and accuracy orders on the regular triangulation of the unit square. The second-order derivatives are approximated by (5.13).

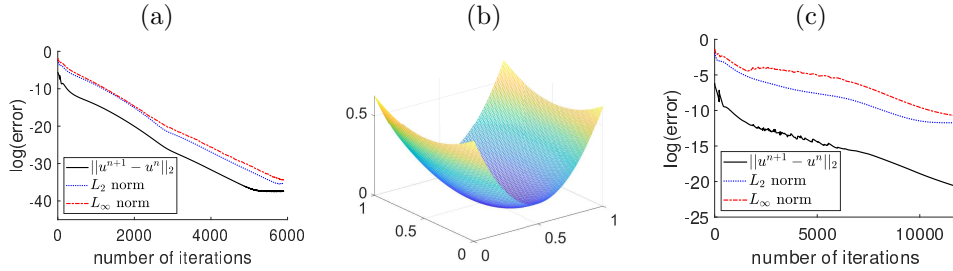


FIG. 3. (Test problem (7.1). Scheme (4.6)-(4.8).) (a): With  $\alpha = 1$ ,  $\varepsilon_1 = \varepsilon_2 = 0$  in both stages, the convergence history on the regular triangulation of the unit square. The second-order derivatives are approximated by (5.13). (b)-(c): The graph of the computed solution and the convergence history on the regular triangulation of the unit square. The second-order derivatives are approximated by (5.13).

568 shown in Figure 2. The numbers of iteration and accuracy orders are shown in Table  
569 1, where the accuracy orders in the  $L_2$  and  $L_\infty$  norms are in general larger than 1.5.  
570 Stopping criterion  $\|u^{n+1} - u^n\| < 10^{-9}$  is used. Since the time step is in the order of  
571  $h^2$ , we expect that the rate of convergence is close to 2. In Table 1, the rate is around  
572 1.8, which is slightly better than our expectation.

573 With the second-order derivatives approximated by (5.19) and (5.20) and scheme  
574 (4.6)-(4.8), we can use a less demanding stopping criterion. Here we use  $\|u^{n+1} -$   
575  $u^n\| < 10^{-7}$ . The numbers of iteration, the errors of approximation, and the rates  
576 of convergence on regular and symmetric meshes of the unit square are shown in  
577 Table 2, which demonstrate that, in general, our algorithm with approximation (5.19)  
578 and (5.20) is first-order accurate, and in comparison with the results based on the  
579 approximation (5.13), the errors based on the approximation (5.19) and (5.20) are  
580 larger and the convergence rates are smaller.

581 For comparison, we also show the results by scheme (4.16)-(4.18) with the second-

	$h$	Iteration	$\ u^{n+1} - u^n\ _2$	$L_2$ error	rate	$L_\infty$ error	rate
(a)	1/16	177	$9.57 \times 10^{-7}$	$9.79 \times 10^{-2}$		$1.69 \times 10^{-1}$	
	1/32	791	$9.98 \times 10^{-7}$	$5.61 \times 10^{-2}$	0.80	$1.19 \times 10^{-1}$	0.51
	1/64	3360	$9.97 \times 10^{-7}$	$3.12 \times 10^{-2}$	0.85	$8.39 \times 10^{-2}$	0.50
	1/128	17273	$9.99 \times 10^{-7}$	$1.55 \times 10^{-2}$	1.01	$5.86 \times 10^{-2}$	0.52
	$h$	Iteration	$\ u^{n+1} - u^n\ _2$	$L_2$ error	rate	$L_\infty$ error	rate
(b)	1/16	236	$9.72 \times 10^{-7}$	$2.86 \times 10^{-2}$		$7.40 \times 10^{-2}$	
	1/32	1179	$9.98 \times 10^{-7}$	$1.13 \times 10^{-2}$	1.34	$4.53 \times 10^{-2}$	0.71
	1/64	5261	$9.95 \times 10^{-7}$	$7.33 \times 10^{-3}$	0.62	$4.12 \times 10^{-2}$	0.14
		$h$	$L_\infty$ error	rate			
(c)	1/16		$1.61 \times 10^{-1}$				
	1/32		$1.28 \times 10^{-1}$	0.33			
	1/64		$1.09 \times 10^{-1}$	0.23			
	1/128		$8.80 \times 10^{-2}$	0.31			

TABLE 5

(Test problem (7.2). Scheme (4.6)-(4.8).) Numbers of iterations, approximation errors, and accuracy orders with the second-order derivatives approximated by (a) (5.13) and (b) (5.19)-(5.20). (c) shows the  $L_\infty$  errors and accuracy orders from [30].

582 order derivatives approximated by (5.13). Since the boundary condition is compatible,  
 583 we use a large  $\kappa = 500$ . The number of iteration and accuracy orders are shown in  
 584 Table 3. Its efficiency and accuracy are similar to that of scheme (4.16)-(4.18). If  $\kappa$   
 585 goes to infinity, scheme (4.16)-(4.18) has an additional stabilization (diffusion) term  
 586 which provides larger error but extra robustness, the same as what is observed by  
 587 comparing Table 1(a) and Table 3.

588 Since the exact solution is a quadratic function, its second-order derivatives are  
 589 constants so that the zero Neumann boundary condition on these derivatives is exact.  
 590 With  $\varepsilon = \varepsilon_1 = 0$  and  $h = 1/40$ , the convergence history of scheme (4.6)-(4.8) is shown  
 591 in Figure 3(a). We can see that although approximation (5.13) is a kind of variational  
 592 crime, the error decreases to machine precision.

593 In the second test, we choose  $\alpha = 2$  so that  $u^*$  represents a family of con-centric  
 594 ellipses which vary anisotropically. We apply our algorithm to this problem on the  
 595 unit square with regular meshes. The number of iterations necessary to satisfy the  
 596 stopping criterion and the corresponding approximation error accuracy is shown in  
 597 Table 4. The graph of the computed solution and the related convergence history are  
 598 shown in Figure 3(b)-(c).

599

600 **7.2. Example 2.** In the second example, we consider a problem with the exact  
 601 solution

602 (7.2) 
$$u = -\sqrt{1 - x_1^2 - x_2^2},$$

603 which is a part of the unit sphere, and the corresponding Gauss curvature is con-  
 604 stant:  $K = 1$ . The computational domain is chosen to be half of the unit disk,  
 605  $\Omega = \{(x_1, x_2) | x_1 \geq 0, x_1^2 + x_2^2 \leq 1\}$ . Accordingly, the boundary condition is given as

606 (7.3) 
$$g = \begin{cases} 0, & x_1 > 0, \\ -\sqrt{1 - x_2^2}, & x_1 = 0. \end{cases}$$

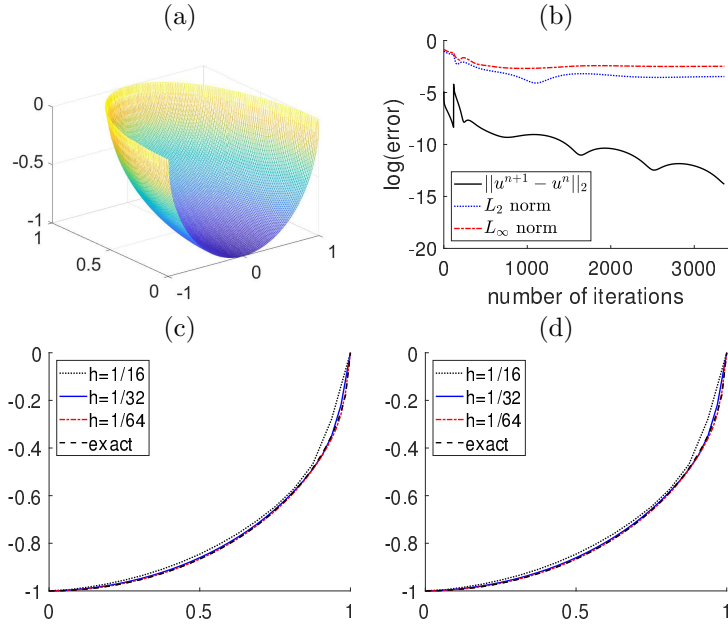


FIG. 4. (Test problem (7.2). Scheme (4.6)-(4.8)) (a) The graph of the solution with  $h = 1/64$ , where the second-order derivatives are approximated by (5.13). (b) The convergence history of (a). (c)-(d): Graphs of the restrictions of the numerical solutions to the line  $x_1 = 0$  with different  $h$ 's. (c) the second-order derivatives approximated by (5.13) and (d) the second-order derivatives approximated by (5.19)-(5.20).

607 This problem is interesting since the gradient of the exact solution along the  
 608 boundary where  $x_1 > 0$  is infinite (a more challenging problem is solved in Sup-  
 609 plementary materials ??). This problem is also solved in [30]. Since the first-order  
 610 derivatives are infinite along a part of the boundary, we have to use the regularized  
 611 approximation (5.5) for the first-order derivatives; otherwise our solution will blow  
 612 up. We use  $\varepsilon = h$ ,  $\varepsilon_1 = h^2$ ,  $\Delta t = h^2$ , and the stopping criterion  $\|u^{n+1} - u^n\|_2 < 10^{-6}$ .  
 613 Figure 4(a)-(b) shows the graph of the numerical solution for  $h = 1/64$  and the re-  
 614 lated convergence history with second-order derivatives approximated by (5.13). The  
 615 cross sections of the numerical solutions along the boundary  $x_1 = 0$  with second-order  
 616 derivatives approximated by (5.13) or (5.19)-(5.20) are shown in Figure 4(c)-(d), and  
 617 the convergence of numerical solutions using both approximations is clearly observed.

618 To further quantify both approximations of second-order derivatives, we show  
 619 the numbers of iterations, the  $L_2$ - and  $L_\infty$ - errors, and their corresponding rates of  
 620 convergence in Tables 5(a) and (b). In Table 5, we can see that both approximations of  
 621 the second-order derivatives behave reasonably well. Although the algorithm equipped  
 622 with approximation (5.19)-(5.20) produces smaller errors than the one equipped with  
 623 (5.13), the algorithm with approximation (5.13) is more stable as its convergence  
 624 rate is uniformly about 0.5. As a comparison, we also list the  $L_\infty$ -errors and related  
 625 convergence rates from [30] in Table 5(c). When the mesh is fine enough, our algorithm  
 626 equipped with either approximations produces smaller  $L_\infty$ -errors than that of [30].

627 **7.3. Example 3.** We end this section by considering a problem with no classical  
 628 solution. The curvature is a constant in  $\Omega$ :

629 (7.4) 
$$K = 1/2 \text{ in } \Omega,$$

(a)						
$h$	Iter.	$\ u^{n+1} - u^n\ _2$	$\ \mathbf{p}^n - \mathbf{D}^2 u^n\ _2$	$\frac{\ \mathbf{p}^n - \mathbf{D}^2 u^n\ _2}{\ \mathbf{p}^n\ _2}$	min	$\ \mathbf{p}^n - \mathbf{D}^2 u^n\ _2$ in.
1/20	177	$9.62 \times 10^{-7}$	$4.44 \times 10^{-2}$	$2.35 \times 10^{-2}$	-0.1192	$3.28 \times 10^{-3}$
1/40	672	$9.72 \times 10^{-7}$	$1.80 \times 10^{-1}$	$7.26 \times 10^{-2}$	-0.1263	$5.98 \times 10^{-3}$
1/80	2149	$9.98 \times 10^{-7}$	$4.94 \times 10^{-1}$	$1.67 \times 10^{-1}$	-0.1305	$9.41 \times 10^{-3}$

(b)						
$h$	Iter.	$\ u^{n+1} - u^n\ _2$	$\ \mathbf{p}^n - \mathbf{D}^2 u^n\ _2$	$\frac{\ \mathbf{p}^n - \mathbf{D}^2 u^n\ _2}{\ \mathbf{p}^n\ _2}$	min	$\ \mathbf{p}^n - \mathbf{D}^2 u^n\ _2$ in.
1/20	246	$9.88 \times 10^{-7}$	$4.60 \times 10^{-3}$	$2.43 \times 10^{-3}$	-0.1345	$7.47 \times 10^{-4}$
1/40	695	$9.88 \times 10^{-7}$	$7.53 \times 10^{-2}$	$2.43 \times 10^{-2}$	-0.1359	$4.77 \times 10^{-3}$
1/80	2468	$9.99 \times 10^{-7}$	$3.52 \times 10^{-1}$	$6.82 \times 10^{-2}$	-0.1376	$6.54 \times 10^{-3}$

TABLE 6

(Test problem (7.4). Scheme (4.6)-(4.8).) Numbers of iterations, iteration errors and minimum values. The second-order derivatives are approximated by (a) (5.13) and (b) (5.19)-(5.20).

630 where  $\Omega = [0, 1]^2$ . We use the boundary condition  $g = 0$  on  $\partial\Omega$ . This problem has  
631 no classical solution since  $\det(\mathbf{D}^2 u)$  vanishes on  $\partial\Omega$ . In other words, this problem is  
632 incompatible. In our experiment, we first use scheme (4.6)-(4.8) with  $\varepsilon = \varepsilon_1 = \varepsilon_2 = h^2$   
633 and  $\Delta t = 2h^2$ . The second-order derivatives are approximated by (5.13). The number  
634 of iterations, convergence errors, and minimum values are shown in Table 6. The  
635 graphs and contour of the numerical solution with  $h = 1/80$  are shown in Figure 5  
636 Row 1. The comparisons of the restriction of the numerical solution with different  $h$   
637 along  $x_1 = 1/2$  and  $x_1 = x_2$  are shown in Figure 5 Row 2. Our solution is smooth  
638 and almost convex, except for the region near the corners of the domain.

639 Then we use scheme (4.16)-(4.18) with  $\varepsilon = \varepsilon_1 = \varepsilon_2 = h^2$  and  $\Delta t = 8h^2$  to solve  
640 it. With  $h = 1/80$ , the graph and contour of the computed solution are shown in  
641 Figure 5 Row 3. We can see the boundary value of the computed solution is no  
642 longer constant. At the middle segment on each edge, its value is away from 0 to be  
643 compatible with its interior value. The comparisons of the restriction of the numerical  
644 solution with different  $h$  along  $x_1 = 1/2$  and  $x_1 = x_2$  are shown in the fourth row  
645 of Figure 5. Compared to the graph in the second row of Figure 5, we observe the  
646 deviation of the boundary value from 0. The same problem is solved on an ellipse  
647 domain in Supplementary materials ??.

648 **8. Conclusion.** In this work, we have proposed two operator splitting/mixed  
649 finite-element methods to solve the Dirichlet Minkowski problem in dimension two.  
650 Our algorithms are easy to implement since only a system of PDEs is to be solved  
651 and the basis functions are chosen to be piecewise linear. When the problem has  
652 a classical solution, scheme (4.6)-(4.8) using approximation (5.19)-(5.20) for second-  
653 order derivatives is first-order accurate while using approximation (5.13) it is almost  
654 second-order accurate. For an incompatible problem, scheme (4.16)-(4.18) can adjust  
655 the boundary value of the computed solution to make it compatible with its interior  
656 values. Our algorithm can solve the Minkowski problem on arbitrary shaped domains  
657 and can also solve problems with singularities in the solution gradient. Our algorithm  
658 can be easily extended to high dimensions, which constitutes an ongoing work.

659 **Acknowledgments.** The preparation of this manuscript has been overshadowed  
660 by Prof. Roland Glowinski's passing away. Roland and the authors had intended to  
661 write jointly: most of the main ideas were worked out together and the authors have  
662 done their best to complete them. In sorrow, the authors dedicate this work to his

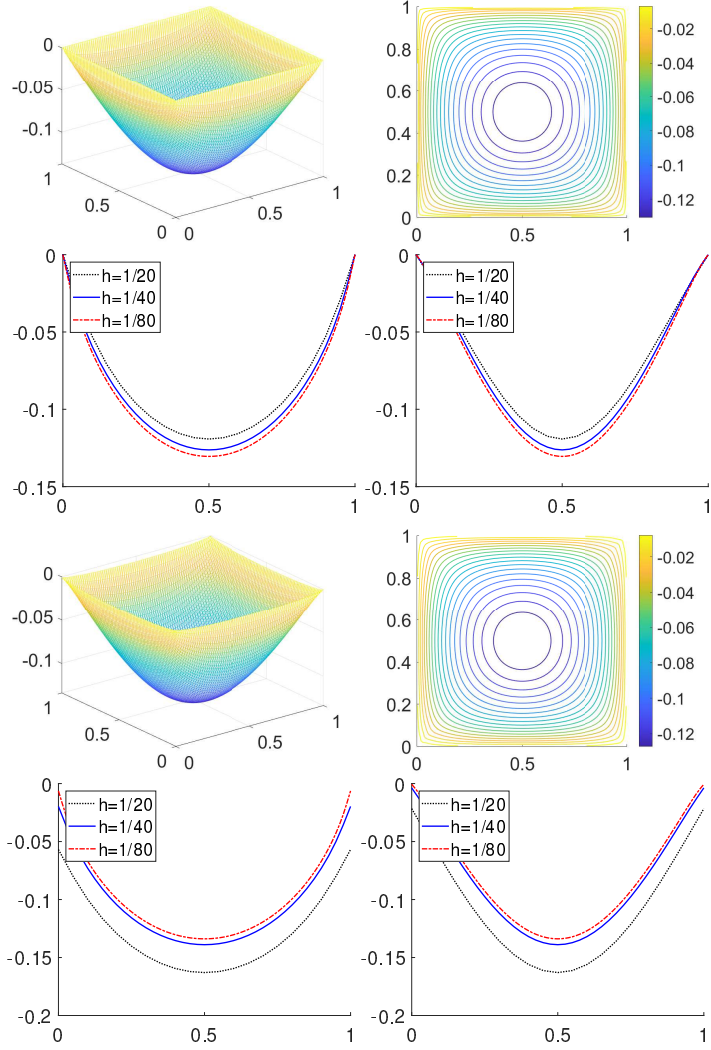


FIG. 5. (Test problem (7.4).) Row 1-2: Scheme (4.6)-(4.8). Row 1: Graphs and contour of the numerical solution with  $h = 1/80$ . Row 2: Graphs of the restrictions of numerical solutions along  $x_1 = 1/2$  (left) and  $x_1 = x_2$  (right) with  $h = 1/20, 1/40$ , and  $1/80$ . Row 3-4: Scheme (4.16)-(4.18.). Row 3: Graphs and contour of the numerical solution with  $h = 1/80$ . Row 4: Graphs of the restrictions of numerical solutions along  $x_1 = 1/2$  (left) and  $x_1 = x_2$  (right) with  $h = 1/20, 1/40$ , and  $1/80$ . The second-order derivatives are approximated by (5.13).

663 memory. Roland's creativity, generosity, and friendship will be remembered.

664

## REFERENCES

665 [1] G. AWANOU, *Standard finite elements for the numerical resolution of the elliptic Monge-Ampère*  
 666 *equation: classical solutions*, IMA Journal of Numerical Analysis, 35 (2014), pp. 1150–1166.  
 667 [2] I. BAKELMAN, *Generalized elliptic solutions of the dirichlet problem for the Monge-Ampère*  
 668 *equations*, in Proc. Symp. Pure Math., AMS, vol. 44, 1986, pp. 1–30.  
 669 [3] I. J. BAKEL'MAN, *The Dirichlet problem for the elliptic  $n$ -dimensional Monge-Ampère equation*  
 670 *and related problems in the theory of quasilinear equations*, in Proceedings of Seminar

on Monge-Ampère Equations and Related Topics, Firenze, 1980, pp. 1–78.

[4] J.-D. BENAMOU AND Y. BRENIER, *A computational fluid mechanics solution to the Monge-Kantorovich mass transfer problem*, Numerische Mathematik, 84 (2000), pp. 375–393.

[5] J. D. BENAMOU, B. D. FROESE, AND A. M. OBERMAN, *Two numerical methods for the elliptic Monge–Ampère equation*, ESAIM: Mathematical Modelling and Numerical Analysis, 44 (2010), pp. 737–758.

[6] S. BRENNER, T. GUDI, M. NEILAN, AND L. SUNG,  *$C^0$  penalty methods for the fully nonlinear Monge–Ampère equation*, Mathematics of Computation, 80 (2011), pp. 1979–1995.

[7] S. C. BRENNER AND M. NEILAN, *Finite element approximations of the three dimensional Monge–Ampère equation*, ESAIM: Mathematical Modelling and Numerical Analysis, 46 (2012), pp. 979–1001.

[8] A. CABOUDSAT, R. GLOWINSKI, AND D. C. SORENSEN, *A least-squares method for the numerical solution of the Dirichlet problem for the elliptic Monge–Ampère equation in dimension two*, ESAIM: Control, Optimisation and Calculus of Variations, 19 (2013), pp. 780–810.

[9] L. CAFFARELLI AND R. GLOWINSKI, *Numerical solution of the Dirichlet problem for a Pucci equation in dimension two. Application to homogenization*, J. Numer. Math., 16 (2008), pp. 185–216.

[10] L. T. CHENG, *Construction of shapes arising from the Minkowski problem using a level set approach*, Journal of Scientific Computing, 19 (2003), pp. 123–138.

[11] S. Y. CHENG AND S. T. YAU, *On the regularity of the solution of the  $n$ -dimensional Minkowski problem*, Communications on Pure and Applied Mathematics, 29 (1976), pp. 495–516.

[12] P. G. CIARLET AND P.-A. RAVIART, *A mixed finite element method for the biharmonic equation*, in Mathematical aspects of finite elements in partial differential equations, Elsevier, 1974, pp. 125–145.

[13] E. J. DEAN AND R. GLOWINSKI, *Numerical solution of the two-dimensional elliptic Monge–Ampère equation with Dirichlet boundary conditions: an augmented Lagrangian approach*, Comptes Rendus Mathématique, 336 (2003), pp. 779–784.

[14] E. J. DEAN AND R. GLOWINSKI, *Numerical solution of the two-dimensional elliptic Monge–Ampère equation with Dirichlet boundary conditions: a least-squares approach*, Comptes Rendus Mathématique, 339 (2004), pp. 887–892.

[15] E. J. DEAN AND R. GLOWINSKI, *An augmented Lagrangian approach to the numerical solution of the Dirichlet problem for the elliptic Monge–Ampère equation in two dimensions*, Electronic Transactions on Numerical Analysis, 22 (2006), pp. 71–96.

[16] E. J. DEAN AND R. GLOWINSKI, *Numerical methods for fully nonlinear elliptic equations of the Monge–Ampère type*, Computer Methods in Applied Mechanics and Engineering, 195 (2006), pp. 1344–1386.

[17] E. J. DEAN AND R. GLOWINSKI, *On the numerical solution of the elliptic Monge–Ampère equation in dimension two: A least-squares approach*, in Partial Differential Equations, Springer, 2008, pp. 43–63.

[18] E. J. DEAN, R. GLOWINSKI, AND T. W. PAN, *Operator-splitting methods and applications to the direct numerical simulation of particulate flow and to the solution of the elliptic Monge–Ampère equation*, in Control and Boundary Analysis, CRC Press, 2005, pp. 1–27.

[19] X. FENG, R. GLOWINSKI, AND M. NEILAN, *Recent developments in numerical methods for fully nonlinear second order partial differential equations*, SIAM Review, 55 (2013), pp. 205–267.

[20] B. D. FROESE AND A. M. OBERMAN, *Convergent finite difference solvers for viscosity solutions of the elliptic Monge–Ampère equation in dimensions two and higher*, SIAM Journal on Numerical Analysis, 49 (2011), pp. 1692–1714.

[21] B. D. FROESE AND A. M. OBERMAN, *Fast finite difference solvers for singular solutions of the elliptic Monge–Ampère equation*, Journal of Computational Physics, 230 (2011), pp. 818–834.

[22] R. GLOWINSKI, *Approximations externes par éléments finis d'ordre un et deux du problème de dirichlet pour  $\delta$* , Topics in numerical analysis I (JJH Miller ed.), (1973).

[23] R. GLOWINSKI, *Numerical Methods for Nonlinear Variational Problems*, Springer Ser. Comput. Phys.(Springer), 1984.

[24] R. GLOWINSKI, *Lectures on Numerical Methods for Non-linear Variational Problems*, Springer Science & Business Media, 2008.

[25] R. GLOWINSKI, *Numerical methods for fully nonlinear elliptic equations*, in 6th International Congress on Industrial and Applied Mathematics, ICIAM, vol. 7, 2009, pp. 155–192.

[26] R. GLOWINSKI, *Variational Methods for the Numerical Solution of Nonlinear Elliptic Problems*, vol. 86, SIAM, Philadelphia, PA, 2015.

[27] R. GLOWINSKI, S. LEUNG, H. LIU, AND J. QIAN, *On the numerical solution of nonlinear eigenvalue problems for the Monge–Ampère operator*, ESAIM: Control, Optimisation and

Calculus of Variations, 26 (2020), p. 118.

[28] R. GLOWINSKI, H. LIU, S. LEUNG, AND J. QIAN, *A finite element/operator-splitting method for the numerical solution of the two dimensional elliptic Monge–Ampère equation*, Journal of Scientific Computing, (2019), pp. 1–47.

[29] R. GLOWINSKI, S. OSHER, AND W. YIN, *Splitting Methods in Communication, Imaging, Science, and Engineering*, Springer, 2016.

[30] B. HAMFELDT, *Convergent approximation of non-continuous surfaces of prescribed Gaussian curvature*, Communications on Pure & Applied Analysis, 17 (2018), pp. 671–707.

[31] L. LAMBERG, *On the Minkowski problem and the lightcurve operator*, dissertation, Academia Scientiarum Fennica, Series A. I., 1993.

[32] L. LAMBERG AND M. KAASALAINEN, *Numerical solution of the Minkowski problem*, Journal of Computational and Applied Mathematics, 137 (2001), pp. 213–227.

[33] H. LEWY, *A priori limitations for solutions of Monge–Ampère equations*, Transactions of the American Mathematical Society, 37 (1935), pp. 417–434.

[34] H. LEWY, *On differential geometry in the large. I. Minkowski’s problem*, Transactions of the American Mathematical Society, 43 (1938), pp. 258–270.

[35] P. L. LIONS, *Sur les équations de Monge–Ampère*, Archive for Rational Mechanics and Analysis, 89 (1985), pp. 93–122.

[36] J. J. LITTLE, *An iterative method for reconstructing convex polyhedra from external Gaussian images*, in AAAI, 1983, pp. 247–250.

[37] J. J. LITTLE, *Recovering shape and determining attitude from extended Gaussian images*, PhD thesis, University of British Columbia, 1985.

[38] H. LIU, R. GLOWINSKI, S. LEUNG, AND J. QIAN, *A finite element/operator-splitting method for the numerical solution of the three dimensional Monge–Ampère equation*, Journal of Scientific Computing, 81 (2019), pp. 2271–2302.

[39] H. LIU, S. LEUNG, AND J. QIAN, *An Efficient Operator-Splitting Method for the Eigenvalue Problem of the Monge–Ampère Equation*, Communications in Optimization Theory, 2022 (2022), pp. 1–22.

[40] G. LOEPER AND F. RAPETTI, *Numerical solution of the Monge–Ampère equation by a Newton algorithm*, C. R. Acad. Sci. Paris, Ser. I, 340 (2005), pp. 319–324.

[41] H. MINKOWSKI, *Allgemeine Lehrsätze über die konvexen Polyeder*, in Ausgewählte Arbeiten zur Zahlentheorie und zur Geometrie, Springer, 1989, pp. 121–139.

[42] H. MINKOWSKI, *Volumen und Oberfläche*, in Ausgewählte Arbeiten zur Zahlentheorie und zur Geometrie, Springer, 1989, pp. 146–192.

[43] B. MOHAMMADI, *Optimal transport, shape optimization and global minimization*, Comptes Rendus Mathématique, 344 (2007), pp. 591–596.

[44] L. NIRENBERG, *The Weyl and Minkowski problems in differential geometry in the large*, Communications on Pure and Applied Mathematics, 6 (1953), pp. 337–394.

[45] A. V. POGORELOV, *Regularity of a convex surface with given Gaussian curvature*, Matematicheskii Sbornik, 73 (1952), pp. 88–103.

[46] A. V. POGORELOV, *The Minkowski multidimensional problem*, in Scripta Series in Mathematics, J. Wiley, 1978.

[47] H. SCHAEFFER AND T. Y. HOU, *An accelerated method for nonlinear elliptic PDE*, Journal of Scientific Computing, 69 (2016), pp. 556–580.

[48] N. S. TRUDINGER AND J. I. E. URBAS, *The Dirichlet problem for the equation of prescribed Gauss curvature*, Bulletin of the Australian Mathematical Society, 28 (1983), pp. 217–231.

[49] N. S. TRUDINGER AND X. J. WANG, *The Monge–Ampère equation and its geometric applications*, Handbook of Geometric Analysis, 1 (2008), pp. 467–524.

[50] J. I. E. URBAS, *The equation of prescribed Gauss curvature without boundary conditions*, Journal of Differential Geometry, 20 (1984), pp. 311–327.

[51] J. I. E. URBAS, *Global Hölder estimates for equations of Monge–Ampère type*, Inventiones Mathematicae, 91 (1988), pp. 1–29.

[52] J. I. E. URBAS, *Boundary regularity for solutions of the equation of prescribed Gauss curvature*, Annales de l’Institut Henri Poincaré (C) Non Linear Analysis, 8 (1991), pp. 499–522.